REPORT DOCUMENTATION PAGE

AFRL-SR-BL-TR-02-

0070

1. REPORT DATE (DD-MM-YYYY)	2. REPORT TYPE	3. DATES COVERED (From - To)
01-Feb-2002	Final Technical	02-Jan-1998 To 01-Jan-2001

4. TITLE AND SUBTITLE

Materials for Optical Routers, Signal Processors, and Memories Based on Persistent Spectral Hole Burning

5a. CONTRACT NUMBER

5b. GRANT NUMBER
F49620-98-1-0171

5c. PROGRAM ELEMENT NUMBER

5d. PROJECT NUMBER

5e. TASK NUMBER

5f. WORK UNIT NUMBER

6. AUTHOR(S)

Cone, Rufus L., Professor of Physics
Physics Department, Montana State University, Bozeman, MT

7. PERFORMING ORGANIZATION NAME(S) AND ADDRESS(ES)

Office of Grants and
Contracts
Montana State University
Bozeman, MT 59717

8. PERFORMING ORGANIZATION REPORT NUMBER

9. SPONSORING / MONITORING AGENCY NAME(S) AND ADDRESS(ES)

AFOSR/NE
801 North Randolph Street
Arlington, VA 22203-1977

10. SPONSOR/MONITOR'S ACRONYM(S)

11. SPONSOR/MONITOR'S REPORT NUMBER(S)

12. DISTRIBUTION / AVAILABILITY STATEMENT

DISTRIBUTION STATEMENT A
Approved for Public Release
Distribution Unlimited

AIR FORCE OFFICE OF SCIENTIFIC RESEARCH (AFOSR)
NOTICE OF TRANSMITTAL DTIC. THIS TECHNICAL REPORT
HAS BEEN REVIEWED AND IS APPROVED FOR PUBLIC RELEASE
LAW AFR 190-12. DISTRIBUTION IS UNLIMITED.

13. SUPPLEMENTARY NOTES

14. ABSTRACT

Optical signal processing devices using spectral hole burning were demonstrated, including an optical header decoder for packet switching and tests of signal correlator fidelity and phase-shift-keyed codes. New hole burning materials were developed and characterized. Performance improvements of the materials include (a) multi-GHz bandwidths for signal processors, (b) increased capacity and storage time for data storage, (c) improved frequency stability for lasers stabilized to spectral hole frequency references. The new materials include Er^{3+} compounds for 1.5 micron communications bands, Tm^{3+}, Pr^{3+}, Eu^{3+}, and Tb^{3+} compounds, mostly in oxide crystal hosts. Tb^{3+} compounds were characterized for photon gated persistent spectral hole burning. Electron photoemission spectroscopy was used to determine important relationships between ion levels and host bands and to develop gated persistent hole burning materials; those results have substantial corollary impacts on robustness and efficiency of solid-state laser materials, phosphors for displays, and scintillators for imaging. For all crystal materials – of any symmetry –angular orientation and polarization has been optimized for signal fidelity and fastest transient response in hole burning devices. There were 7 published journal articles, 16 invited presentations, 36 contributed presentations, and participation on 7 conference committees. The project involved five graduate students, nine undergraduates, three postdocs and scientists, along with the PIs. Other AFOSR-supported groups use these materials; Scientific Materials Corp. sells the materials.

15. SUBJECT TERMS

spectral hole burning, optical material, rare earth, photon echo, optical correlator, laser, optical, spectroscopy, coherent transient, frequency standard

16. SECURITY CLASSIFICATION OF:			17. LIMITATION OF ABSTRACT	18. NUMBER OF PAGES	19a. NAME OF RESPONSIBLE PERSON
a. REPORT	b. ABSTRACT	c. THIS PAGE			19b. TELEPHONE NUMBER *(include area code)*

20020305 120

Final Technical Report

for 02 January 1998 to 01 January 2001

submitted by

Rufus L. Cone, Principal Investigator
Physics Department
Montana State University
Bozeman, MT 59717
Telephone: 406-994-6175
FAX: 406-994-4452
Internet: cone@montana.edu

on

AFOSR-DEPSCoR Contract Number F49620-98-1-0171

MATERIALS FOR OPTICAL ROUTERS, SIGNAL PROCESSORS, AND MEMORIES BASED ON PERSISTENT SPECTRAL HOLE BURNING

submitted to

Dr. Kent Miller, Program Manager
AFOSR/NE
801 North Randolph Street, Room 732
Arlington, VA 22203-1977

SUMMARY OF OBJECTIVES AND ACCOMPLISHMENTS

Optical memories and optical signal processing based on spectral hole burning (SHB) and optical coherent transients can dramatically increase optical data storage density, provide a new range of signal-processing devices, and provide enhanced timing accuracy in phased-array radar. The search for new optical materials for these SHB applications, evaluation of the SHB materials' dynamic and static properties, studies of the ultimate limits on SHB material performance, and demonstrations of SHB correlator devices for router applications constitute the research that we carried out under this *AFOSR* grant. We worked to understand the atomic-scale mechanisms that determine material performance, emphasizing parameters relevant to device development. Attention was focused on rare earth doped materials; material systems for photon-gated SHB were also explored both by hole burning experiments and electron photoemission spectroscopy. We designed a range of new crystal materials containing Eu^{3+}, Pr^{3+}, Tm^{3+}, Tb^{3+}, and Er^{3+} ions and optimized their hole burning and coherent transient properties. Crystal composition and rare earth ion concentration were tailored to specific device needs. Improvements of performance parameters, often by more than an order of magnitude, were achieved for these materials at a variety of wavelengths where diode laser sources make new materials especially important. In the case of Er^{3+}, we demonstrated device applications based on spectral hole burning and coherent transient applications in the 1.5 μm optical communications bands. Going beyond specific materials, we made a fundamental analysis of crystal symmetry that can guide the choice and design of all future materials. We also carried out a unique range of photoemission experiments to quantitatively relate the rare earth ion levels to the electronic band structure of the host crystals; that study also improves the design process for solid-state laser materials, display phosphors, and scintillators materials for imaging.

Specific accomplishments included:

1. Demonstrated optical signal processing devices based on SHB, including
   - an optical header decoder for packet switching
   - tests of signal correlator fidelity and phase-shift-keyed codes.
2. New hole burning materials were developed and characterized, with performance improvements including
   - multi-GHz bandwidths for signal processors,
   - increased capacity and data storage time,
   - improved frequency stability for lasers stabilized to spectral hole frequency references and development of improved reference materials.
3. The new hole burning materials include Er^{3+} compounds for 1.5 micron communications bands, Tm^{3+}, Pr^{3+}, Eu^{3+}, and Tb^{3+} compounds, mostly in oxide crystal hosts.
4. Eight Tb^{3+} compounds were characterized for photon gated persistent spectral hole burning. Hole burning at 489 nm was recorded at high resolution.
5. To allow intelligent design of materials for gated spectral hole burning, electron photoemission spectroscopy was used to determine important relationships between ion levels and host bands and to develop gated persistent hole burning materials; those results have substantial corollary impacts on robustness and efficiency of solid-state laser materials, phosphors for displays, and scintillators for imaging.
6. For all crystal materials – of any symmetry – angular orientation and polarization has been optimized for signal fidelity and fastest transient response in hole burning devices.

7. There were 7 published journal articles, 16 invited presentations, 36 contributed presentations, and participation on 7 conference committees.
8. The project involved five graduate students, nine undergraduate students, three postdocs and scientists, along with the two PIs.
9. Other AFOSR-supported groups use these materials we have developed and characterized.
10. Scientific Materials Corp. of Bozeman, Montana, sells the materials described in this proposal.

State of the art facilities for SHB research and SHB material characterization are available in our laboratory, and further development in experimental and analytical capabilities occurred during this project. We have twenty years experience studying a variety of rare earth activated hole burning materials. Our work at Montana State University was carried out in collaboration with *Scientific Materials Corporation -- an AFOSR SBIR Phase II contractor*, with Roger Macfarlane at IBM Almaden Research Center, with university groups including Dr. M. J. M. Leask at the University of Oxford, UK, and with other groups in the US and France.

We participated in and helped organize the following AFOSR-sponsored Workshops:

- Fourth International Workshop on Applications of Spectral Hole Burning, Montana State University, Bozeman, MT, March 9-11, 1998.
- Fifth International Workshop on Applications of Spectral Hole Burning, Montana State University, Bozeman, MT, March 7-10, 1999.

We participated in the AFOSR Workshop, SRI, Menlo Park, California, May 25, 2000.

ACCOMPLISHMENTS

A. Optical Signal Processing Device Demonstrations – Spatial-Spectral Holographic Correlators

Spatial-spectral holographic (SSH) devices combine spectral hole burning (SHB) with conventional holography to perform real-time memory and signal-processing functions including correlations of signals with arbitrary phase, frequency, and amplitude modulation; moreover, SSH devices can operate at bandwidths greater than 10 GHz (possibly terahertz), can have time-bandwidth products in excess of 10^5, and can potentially enhance optical communications capabilities. These SSH devices are ideally suited to perform correlations with phase-encoded information, are especially suited multi-phase-shift modulation such as quadriphase and binary-phase-shift keyed (QPSK and BPSK) modulation. We have developed eight different erbium-doped insulating crystals having the frequency-selective and coherence properties that are required for providing SSH devices operating within the important 1.5-mm communications window.

Correlators are important in many signal-processing and memory applications such as pattern recognition, database searching, associative memories, data packet address header decoding, and spread spectrum communications.

Demonstration of Real-Time Address Header Decoding for Optical Data Routing at 1536 nm, T. L. Harris, Y. Sun, R. L. Cone, R. M. Macfarlane, and R. W. Equall, Opt. Lett. **23**, 636-638 (1998).

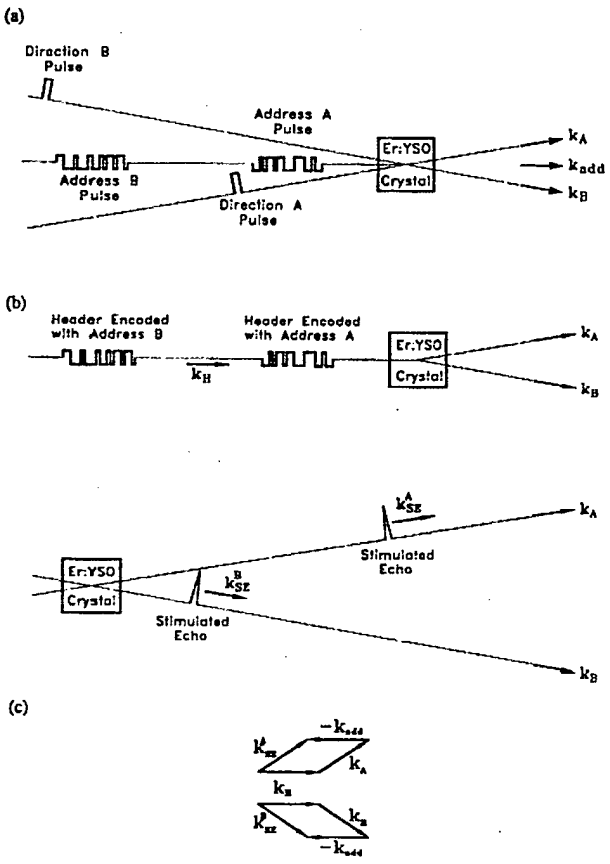

Fig. 1 (a) Temporal snapshot of the programming stage. For each header address, one spatial-spectral grating is stored in the crystal by a pair of programming pulses: a bi-phase coded header address and a brief direction pulse. (b) Temporal snapshots of the processing stage. Headers coded with the addresses produce stimulated photon echoes in the spatial output channels corresponding to the directions programmed into the gratings by the brief direction pulses. (c) Phase matching diagrams determining the wavevectors of the output stimulated photon echoes.

We demonstrated real-time decoding of 20-bit bi-phase coded address header pulses using stimulated photon echoes in a phase-matched crossed-beam configuration. This is one of the functions required for coherent transient optical data routing, packet switching, and signal processing in communications systems and other applications. The active medium used was single crystal Y_2SiO_5 doped with Er^{3+}, which provides an operating wavelength of 1536 nm. We first developed the Er^{3+}:Y_2SiO_5 material and have continued to refine it. The advantages of optical packet switching are well documented and include fast data routing in the wavelength and space domains and transparency to packet bit rate and format.

In our demonstration, we programmed a crystal to recognize bi-phase coded address headers and to decode an arbitrary sequence of these headers, resulting in spatially-discriminated optical output pulses. Each output pulse could be used to control the routing or switching of the optical data packet or the combined header and data packet in real time, requiring only a compact optical delay.

Address header decoding was performed in two stages. First, the processing crystal was programmed with a distinct SSH grating for each address header by the application of a pair of optical programming pulses as shown in Fig. 1(a). This grating was stored by resonant Er3+ ions associated with the inhomogeneously broadened absorption of the Er^{3+}:Y_2SiO_5 spectral hole burning material. The grating provides a simple way to visualize the stimulated photon echo processing function. In the context of wavelength-division multiplexing, one may also store

independent gratings at other adjacent wavelengths in the absorption profile. In this demonstration, we programmed the crystal for two distinct bi-phase coded address headers labeled A and B and two corresponding output directions $\mathbf{k}_A$ and $\mathbf{k}_B$. The bi-phase coded address programming pulse for channel A propagated in the $\mathbf{k}_{add}$ direction and was applied to the crystal just prior to the brief direction programming pulse that propagated along $\mathbf{k}_A$. The direction programming pulse was used to associate the $\mathbf{k}_A$ direction with address header A through the standard stimulated photon echo phase matching conditions of Fig. 1 (c). The convolution of the address pulse and its brief direction pulse formed a spatial-spectral grating that the crystal stored for a time given by the stimulated photon echo lifetime of the material which is about a millisecond in this case but which could be many orders of magnitude longer in materials using a different hole burning mechanism. The second grating, containing address B and its associated echo output direction $\mathbf{k}_B$ was programmed in the same manner as shown in Fig 1 (a).

The header processing stage is shown schematically in Fig. 1 (b). Headers propagated along the $\mathbf{k}_H \equiv \mathbf{k}_{add}$ direction, and each header generated stimulated photon echo output signals following interaction with each stored grating. The phase matching conditions shown in Figure 1(c) predict the emission directions $\mathbf{k}_A$ and $\mathbf{k}_B$ of the individual echoes. The shape of the stimulated echo is determined by the cross-correlation of the header pulse with the convolution of the address and direction programming pulse pair stored in each grating. Cross-correlation calculations predict that the echo produced along $\mathbf{k}_A$ by interaction of an A header with the A grating is dominated by a relatively strong narrow (~ 100 ns duration, one bit wide) central pulse and side lobes more than an order of magnitude weaker. In addition, calculations predict that the unwanted cross-talk echo produced along kB, when header A interacts with grating B has no strong central peak but just weak side lobes. With optimized codes, the cross-correlation between headers can be minimized, thus minimizing the inevitable cross-talk echo. Processing of B code headers proceeded analogously.

The apparatus we used included an external cavity diode laser (ECDL) coupled into an erbium doped fiber amplifier (EDFA). An arbitrary waveform generator was programmed to produce two distinct 20__bit $\pm\pi/2$ bi-phase coded address header pulses A (--+--+++---++-++-+--) and B (-++-++-+--+---+---++) of 2 ms total duration each (100 ns/bit).

A representation of the temporal ordering (ABBABABA) of the 2 ms headers at 9 ms intervals is shown in Fig. 2 (a). Single shot data demonstrating header decoding are given in Fig. 2 (b), which shows the output of the A and B photodiodes. Stimulated photon echoes of 100 ns duration (the bit duration, as mentioned earlier) occur on each channel 3 μs after a correspondingly coded header passes through the crystal. Cross-talk in the form of weaker stimulated photon echo signals in the opposite channel was observed. This was due to the use of unoptimized header address codes, and it demonstrates the need to devise codes that minimize cross-correlation between different headers.

In this signal processing application there are several relevant time scales. During the programming step, coherence (determined by T_2) is only required during one header/direction pulse pair, and ideally the pulse pairs should be separated by more than T_2. Typical values of T_2 for rare earth doped crystals are in the range of 1 - 100 microseconds. In the processing step, the stimulated photon echo decay places an upper limit on the length of the header pulse train that

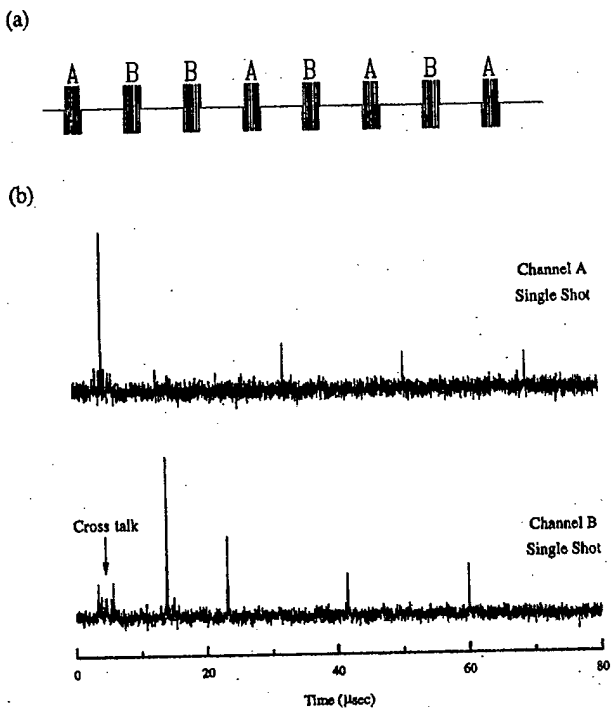

Fig. 2 (a) Representation of the header sequence in the processing stage, showing temporal ordering, spacing and bi-phase coding of the header pulses. (b) Single shot stimulated photon echoes detected during the header processing stage. Echoes are detected on channel A or B at a 3 μs delay after the application of the corresponding header; this delay is determined during the programming stage by the separation of the header

can be processed before reprogramming is required. Different applications will require different time scales; for example in some cases one may want continuous routing with a fixed program and in others one may wish to reprogram rapidly. In the implementation described here, the stimulated echo lifetime is ~1 ms and T_2 is ~150 μs at the field of 8 kG. The stimulated photon echo decay time depends on the mechanism for spectral hole burning and can be as long as hours or days in materials with a persistent hole burning mechanism. In addition, photon-gated materials are known for other wavelength regions in which non-destructive readout is obtained.

Spatial-Spectral Holographic Correlator at 1536 nm Using 30-Symbol Quadriphase- and Binary-Phase-Shift Keyed Codes, T. L. Harris, Y. Sun, W. R. Babbitt, R. L. Cone, J. A. Ritcey, and R. W. Equall, Opt. Lett. **25**, 85-87 (2000).

Extending the work described above, we used more sophisticated codes. We also tested the fidelity of the signal processing output.

Optical 30-symbol quadriphase-shift keyed (QPSK) and binary-phase-shift keyed (BPSK) codes were processed in a spatial-spectral holographic correlator with the Er^{3+}:Y_2SiO_5 spectral hole-burning material operating at 1536 nm in the important 1550-nm communications band. The results demonstrated the unusual ability of spatial-spectral holographic correlators to process QPSK codes and BPSK codes with the same apparatus. The high-fidelity correlations produced by this optical coherent transient device exhibited the low sidelobe characteristics expected for the codes used.

The paper cited above reports processing QPSK and BPSK codes, 30 symbols in length, using the $Er^{3+}:Y_2SiO_5$ SHB material at 1.5 μm; excellent signal fidelity was demonstrated. We believe that these are the only SSH-based correlations that use QPSK codes and that this was the maximum number of symbols achieved for SSH correlations.

The phase-shift keyed codes used as model systems for SSH correlator fidelity studies had previously been selected by very fast simulated re-annealing by minimizing the aperiodic autocorrelation and cross-correlation sidelobes. They were developed for direct sequence-spread spectrum communication, which is desirable for noncentralized, multiple access, coherent optical communication with added security. Direct sequence-spread spectrum communication implementations rely on the correlation properties of coded spread spectrum signals, and in rf links they typically take the form of BPSK modulation.

QPSK codes are more desirable than BPSK in broader contexts, because increasing the number of symbols in the phase alphabet increases the effective information bit rate for a fixed symbol rate and improves security. Increasing the phase alphabet also allows one to trade off sidelobe levels for a larger family of orthogonal codes. At multi-GHz rates, real-time correlation of codes with a phase alphabet of greater than two characters is not possible with current electronic techniques. SSH-based correlators, however, are ideally suited to this task because of their inherent phase sensitivity and bandwidth.

The SSH correlations are performed in two stages. First, the SHB medium is programmed with an SSH grating by application of an optical programming pulse pair. The first of these pulses, the pattern pulse, contains the code that the correlator is being programmed to recognize. The second pulse, the brief reference pulse, is spectrally flat over the bandwidth of the pattern pulse. The pattern and reference pulses, with a combined duration of less than the SHB material's phase memory lifetime, interfere to form a spatial-spectral population grating in the inhomogeneously broadened absorption line in $Er^{3+}:Y_2SiO_5$. This grating contains the product of the Fourier transforms of the two programming pulses and can persist up to the duration of the upper-state lifetime.

In the second stage, the stored grating can process an optical data stream that contains an arbitrary sequence of codes. The amplitude of the stimulated photon echo output is given by the cross correlation of the pattern pulse with the data stream convolved with the reference pulse.1 Because the correlation process takes place entirely within the SHB medium, an SSH correlator can be quite simple, requiring only the SHB crystal, optics, cryogenics, and, for Er^{3+} materials, a small magnet.

In eight separate experiments we used four distinct codes, two QPSK and two BPSK, to generate correlation echoes. We programmed the SHB medium to recognize one such code and used the resultant stored grating to process another code. This produced correlation echoes that were either autocorrelations or cross correlations, depending on whether a replica of the programmed code or an orthogonal code from the same phase-shift keyed family was processed.

The correlator consists of a 0.001% Er^{3+}:Y_2SiO_5 crystal mounted between button-sized NdFeB permanent magnets, providing a magnetic field of $H_0 \sim 2.5$ kG. The crystal and the magnets resided in a 1.5-K cryostat. For these conditions, the coherence lifetime was ~70 μs and the upper-state lifetime was ~10 ms. To examine correlator fidelity, we modulated the output of an external cavity diode laser coupled into an erbium fiber amplifier by using an acousto-optic modulator to produce the programming pulses and data stream. The modulated laser beam was focused to a beam waist radius $w_0 = 100$ μm in the crystal and had nominal peak power of 8 mW. An arbitrary waveform generator synthesized the electrical drive for the acousto-optic modulator and controlled both the phase and the amplitude of the optical beam. The arbitrary waveform generator was programmed to produce the 100-ns/symbol, 3-ms-duration codes.

The QPSK code family was A(00001200102313211031301303230) and B(22322301210333201002021233023). The BPSK code family was A(01100011010001110100100100111) and B(01000100000001110010101110000). Here each number m in the parentheses represents a symbol from the M-PSK (M=4 is QPSK and M=2 is BPSK) phase alphabet AM = [exp(i2πm/M), m = 0, …, M-1]. A reference pulse (area, 0.16π) of 100 ns duration followed the end of each pattern pulse (area, 0.04π/symbol) by 6 μs in these tests. The programming and processing stages were separated by 100 μs, limited by material spectral diffusion, in this demonstration.

Correlation echoes were detected on an InGaAs photodiode whose output was fed into a digitizing oscilloscope for single-shot signal capture. Figure 3 shows a selected single-shot QPSK autocorrelation echo and demonstrates the sharp contrast between the central lobe and sidelobes.

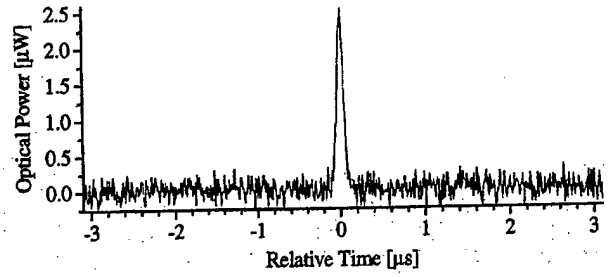

Fig. 3. Single-shot autocorrelation echo for QPSK code A. There is spectacular contrast between the sharp central lobe and the low sidelobes, which are at the level of the photodiode noise floor.

Faithful correlation of the codes by SSH techniques requires that the laser frequency jitter over the interval between the programming and processing stages be much less than the reciprocal of the pattern pulse duration. The low bandwidth modulator that we used mandated 3-ms pattern pulses, for which laser stability of the order of 30 kHz is required. The frequency jitter of the laser used was of the order of hundreds of kilohertz on this time scale and caused severe distortion on most of the single-shot correlations. Thus, criteria were established for selecting correlation single shots that were not significantly influenced by laser frequency jitter. For autocorrelations we selected single shots based on central-lobe intensity. For cross-correlation echo experiments, for which the weak sidelobes did not provide suitable selection criteria, a separate, simultaneous, stimulated echo experiment was performed in a different part of the crystal. The stimulated echo produced in this simultaneous test required the same laser stability as the correlation echoes. We thus used the intensity of the stimulated echo to select

single-shot cross-correlation echoes whose fidelity was not influenced significantly by laser jitter.

We performed numerical simulations of the optical Bloch equations to model the interaction of the optical programming pulses and data stream with the SHB medium. The simulator used assumes a uniform spatial intensity profile of the optical beam in the crystal. The simulation also assumes that the duration of the programming pulse sequence is small compared with the material coherence lifetime. We simulated autocorrelations and cross-correlations for both the QPSK and BPSK code families, using the same approximate pulse areas as in the experiments.

Complete experiment and simulation results are presented in Figs. 4 and 5. The experimental traces are the average of 100 selected single shots with the photodetector background subtracted. This signal averaging resolved the correlation echo sidelobes from the photodetector noise floor and permitted examination of signal fidelity. All correlations, experimental and simulated, have been normalized to the autocorrelation central lobe of that phase-shift keyed family. It can be seen that the experimentally obtained correlation echoes are in excellent quantitative agreement with the simulated signals. The cross correlations exhibit low intensity at the expected autocorrelation-central-lobe arrival time, making them well suited for a system that uses threshold detection.

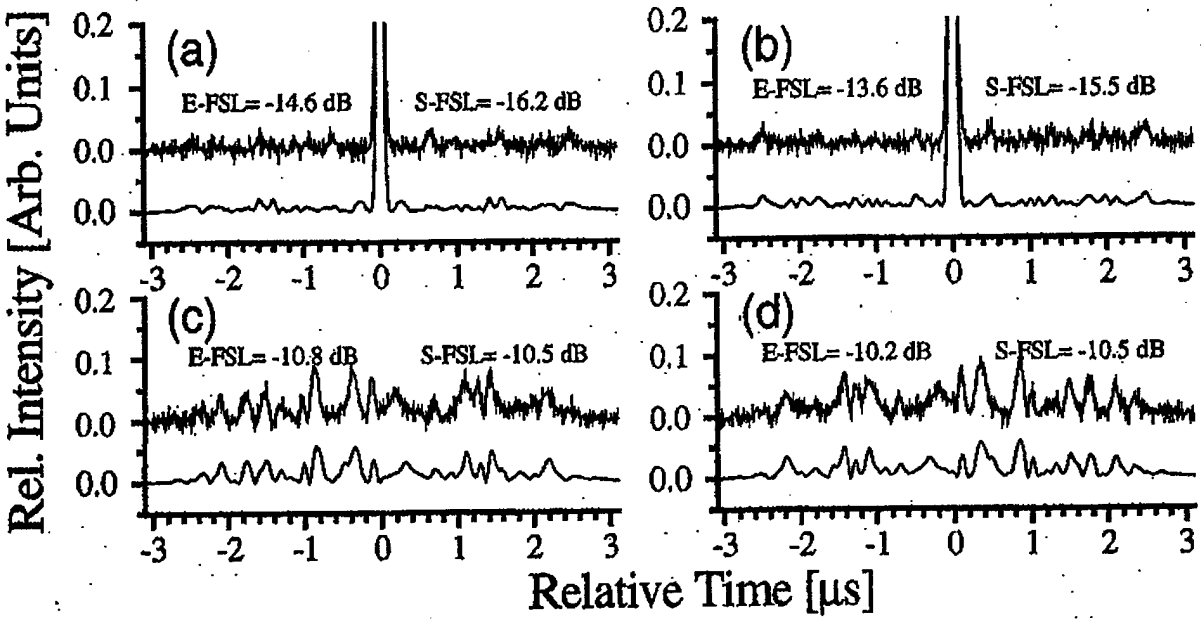

Fig. 4. QPSK correlation results. Top and bottom traces in each graph are experiment and simulation, respectively. Simulation has negative offset in all cases to allow for distinction between traces, and identical scales have been chosen for sidelobe comparison. (a), (b) Autocorrelations for QPSK codes A and B, respectively; (c), (d) cross correlations between QPSK codes.

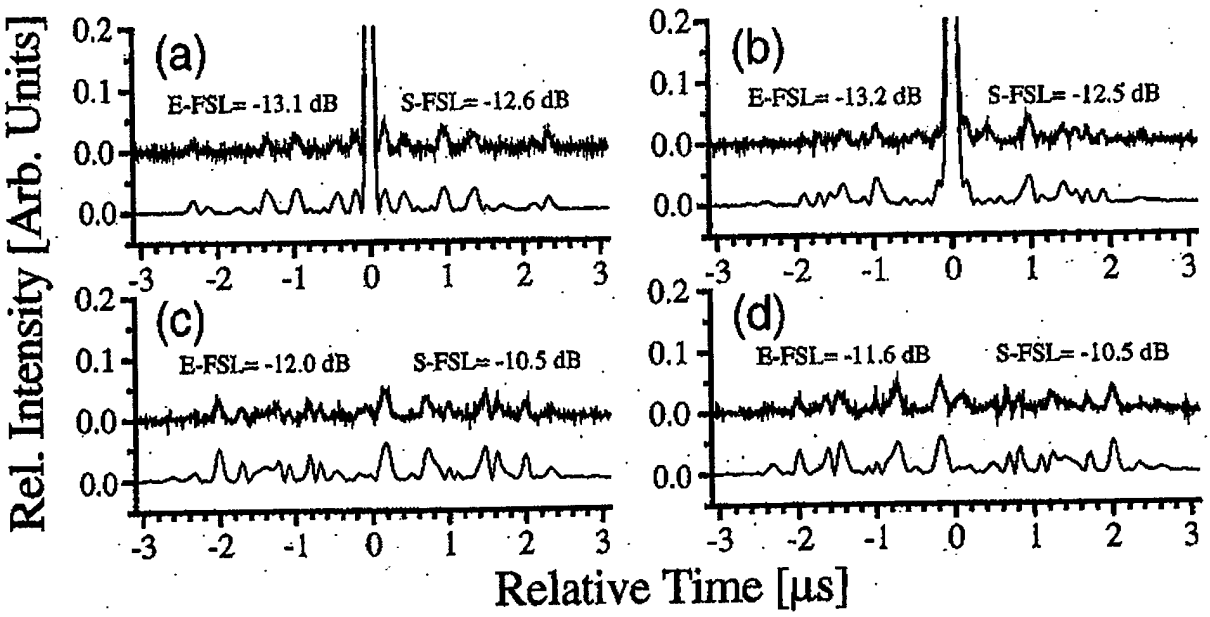

Fig. 5. BPSK correlation results: (a), (b) for autocorrelations; (c), (d) for cross correlations, as in Fig. 4.

Fractional sidelobes (FSL's) are a metric used to evaluate the relative performance of a family of codes and can be thought of as a measure of the contribution to the systematic noise from the codes used. For the QPSK codes the autocorrelation FSL is –16.5 dB and the cross-correlation FSL is –13.9 dB. For the BPSK codes the FSL for both the autocorrelation and the cross-correlation is –14.0 dB. The FSL's for the experimental and simulated (E-FSL and S-FSL) correlations are calculated by taking the ratio of the integrated intensities of the maximum correlation sidelobe and the autocorrelation central lobe. The E-FSL and S-FSL values for each autocorrelation and cross-correlation accompany the data in Figs. 4 and 5.

The slight mismatches between the mathematical correlation function FSL values and those obtained through simulation are expected, not only because these quantities are defined differently, but also because an experimentally unrealizable, delta function reference pulse was used in calculating the mathematically ideal FSL's. The sidelobe mismatch between experimental and simulated correlations can be explained by the distortion of the excitation pulses caused by limited modulator bandwidth, which also contributed to minor distortion of the correlation echoes. Pulse propagation and beam profile effects complicate estimation of experimental pulse areas, and the medium behaves nonlinearly owing to coherent saturation when sufficiently large pulse areas are used. Simulations with various pulse areas suggest that even the relatively small pulse areas used can produce some saturation. In spite of these mechanisms that degrade signal fidelity in a SSH correlator, we have observed excellent fidelity. To more fully exploit the bandwidth capabilities of our SHB materials, we are investigating methods and apparatus for demonstration of multi-gigahertz correlators whose performance will not be laser- or modulator-limited.

In summary, we have demonstrated optical correlations of 30-symbol QPSK and BPSK codes optimized for direct sequence spread spectrum communications in an SSH correlator, using the Er^{3+}:Y_2SiO_5 SHB medium. The operating wavelength is in the important 1.5-μm communications band, and the correlations demonstrate excellent signal fidelity. We believe that this is the first SSH-based correlation with QPSK codes and the first demonstration of correlations by this time-domain technique with such codes that are greater than 20 symbols in length.

B. Spectral Hole Burning Materials Developed for Specific Applications

To meet the demand for storage, access, and processing of larger and larger amounts of data with ever-increasing speed from remote distances, new devices must be developed. To reach maturity, SHB technology requires a well-coordinated effort on material development. Material development and characterization were primary tasks undertaken in this project, and we were in contact with other SHB device development groups worldwide. Our work was facilitated by close cooperation with SBIR contractor Scientific Materials Corporation of Bozeman, Montana.

Our research on materials for SHB and optical coherent transients included a variety of accomplishments and areas of work. A listing is given here, with more detailed reports following in subsequent sections.

a) New materials specifically for high-density random access optical memories were designed, evaluated, and developed. For example, a study of absorption coefficient α and dynamical properties of Eu^{3+}:Y_2SiO_5 as a function of the Eu^{3+} concentration was completed in support of (1) a PetaByte optical dynamic random access SHB memory device (dubbed SpectRAM) developed by DoD contractor Spectrum Lab at MSU and (2) time domain optical memories being characterized for bit error rate at IBM Almaden Research Center.

b) We continued to refine and characterize a number of practical Er^{3+} material for SHB applications in the important 1.5 μm communications region. These included Er^{3+}:Y_2SiO_5, Er^{3+}:Y_2O_3, Er^{3+}:KTP, and Er^{3+}:$LiNbO_3$. The Er^{3+}:Y_2SiO_5 material enabled our demonstration of optical signal processors discussed above. Demonstration of buffer memories at 1.5 μm is projected.

c) For use with diode lasers in the 790 - 800 nm range, Tm^{3+} materials were characterized and optimized. These materials are used by a group of DoD investigators in a MURI project for generation of true time delays in the context of phased array radar.

d) Atomic-scale material properties were determined for Eu^{3+}, Pr^{3+}, Tm^{3+}, Tb^{3+}, and Er^{3+} ions in many hosts.

e) The interaction mechanisms that establish fundamental limits on material performance were studied. Performance parameters were considered for applications including high-density optical storage and high-speed real-time signal processing.

f) "Photon gated" spectral hole burning material development was carried out. Hole burning experiments and UV spectroscopy focused on eight different Tb^{3+} materials, new crystal hosts, and new ion pair combinations. Other studies focused on Pr^{3+} ions in several hosts.

g) Photoemission experiments also were carried out to optimize photon gating by understanding the position of the tightly bound rare earth energy states relative to the conduction bands and valence bands of the host crystals.

h) Provision of solid state frequency references for stable lasers and optical clocks in communications and computer systems using persistent spectral hole burning is another application of interest to our group. At present stability levels, these lasers are having important applications in SHB signal processing device demonstrations where their stability allows lower power to be used.

i) Our work on materials like Eu^{3+}:Y_2SiO_5 suggests that laser frequency stability to the milli-Hertz scale should be achievable with stabilization to spectral holes. Once we

demonstrate even sub-Hz stability, these lasers can be used as the local oscillators in compact ultimate atomic clock devices, and the vibration insensitivity of lasers stabilized to spectral holes should eliminate the need for stable Fabry-Perot cavities and extreme vibration isolation in such applications. This will extend their applicability.

j) Optimization of symmetry considerations in hole burning and coherent transient materials has led us to a general determination of the optimum propagation and light polarization directions for materials with all crystal symmetries. A patent application has been filed, and the Physical Review referees made special comment on the significance of this work.

Among the general material device parameters that we studied were:

a) Limits on the optical homogeneous line widths Γ_h. These limits arise from
   - population lifetime T_1
   - crystal composition through nuclear and electron spin magnetic effects
   - phonon-induced relaxation
   - lattice structure through the effect of phonons
   - possible disorder modes
   - crystal field level gaps above the lowest energy levels – these gaps affect phonon induced dephasing and
   - laser power-induced dephasing or 'instantaneous spectral diffusion',

b) Dependence of the optical homogeneous Γ_h on active ion concentration, temperature, and magnetic field,

c) Spin-lattice relaxation and spectral diffusion processes affecting spectral-hole lifetime,

d) Limits on hole-writing and reading rates,

e) Spectral hole lifetimes arising from metastable intermediate state lifetimes – important for population storage mechanism, for example in Tm^{3+} compounds,

f) Concentration-dependent dephasing and instantaneous spectral diffusion,

g) Growth-dependent effects arising from oxygen vacancies and paramagnetic impurities,

h) Material band gaps and position of ionic ground and excited states within the band gap for design of photon gating strategies (by ultraviolet and x-ray photoemission spectroscopy), and

i) Two-laser photon gated hole burning – efficiencies and hole widths.

A number of materials were designed jointly with Scientific Materials Corporation and produced in Bozeman for this project. Characterization was carried out at our MSU laboratories.
In addition to the materials prepared by Scientific Materials Corporation of Bozeman, we have studied samples from IBM (Roger Macfarlane), several groups at AT&T Bell Laboratories, Yale (W. P. Wolf, S. Mroczkowski), U. Lyon-France (B. Jacquier), Lawrence Livermore National Laboratory (M. J. Weber), Lawrence Berkeley Laboratory (N. M. Edelstein), M.I.T., CREOL, and others.

Studies of Fundamental Limits on Performance:

As a first step in design and production of the optimum material for specific applications, it is important to understand the mechanisms that establish the fundamental limits on performance. Then tradeoffs in material design may be considered.

In applications of time-domain optical signal processing and memory devices, long optical coherence times (dephasing times) T_2 can be especially important because this time largely determines the length of the data train that can be processed or stored at a fixed frequency and also affects the memory storage capacity.

Our accomplishments include studies on Eu^{3+}, Pr^{3+}, and Er^{3+}-doped yttrium silicate materials that have allowed us to demonstrate the narrowest homogeneous optical lines ever observed for each of these ions and the narrowest homogeneous optical lines ever observed in any solids regardless of composition. With these materials, we have significantly improved homogeneous optical coherence times – having recorded millisecond-scale values for each ion. For Er^{3+}:Y_2SiO_5, we have reached optical line widths of Γ_h = 78 Hz, and for Eui^{3+}:Y_2SiO_5, we have reached 122 Hz.

Eu^{3+}:Y_2SiO_5 Materials for Dense Optical Memories

Detailed site-selective spectroscopy has been performed on the $^7F_0$ to $^5D_0$ transition of Eu^{3+} in Eu^{3+}:Y_2SiO_5. To optimize this material for memory applications at Spectrum Lab and IBM Almaden Research Center, our studies on this material have been extended to higher Eu^{3+} concentrations and to higher temperatures ranging from 2 K to 300 K. New samples for these experiments were prepared by Scientific Materials with Eu^{3+} doped at 0.01%, 0.1%, 0.5%, and 1% atomic concentrations. Measurements carried out included time-domain optical dephasing and homogeneous linewidths, fluorescence lifetime, spectral hole lifetime, inhomogeneous linewidth, and anisotropic absorption coefficients for both of the two crystallographically inequivalent Eu^{3+} sites. Analysis of $^5D_0$ emission also allowed the ^7F_J level structures to be determined to assess the potential for applications using those levels and infrared light.

Absorption strength for the optical transition determines the thickness of the optical material required in a memory system. The absorption coefficients of the $^7F_0$ - $^5D_0$ transition for each site were measured at 2 K and room temperature. They were found to be very anisotropic and strongly polarization dependent, even in this very low symmetry crystal.

Measured values of the inhomogeneous linewidth for site 1 increased from Γ_{inh} = 600 MHz to Γ_{inh} = 32 GHz as concentration increased from 0.01% to 1% and site 2 increased from 500 MHz to 39 GHz as shown in Table I below. This dramatic increase in inhomogeneous linewidth indicated that the increasing Eu^{3+} concentration induced significant strain and disorder in the crystals.

Although the integral of the absorption coefficient α increased proportional to the concentration as expected, the peak absorption coefficient remained nominally constant as concentration increased. The strongest absorption was along D1 for site 1 and along b for site 2, though it is only slightly weaker along D1 for site 2. The D1 polarization can be used for applications where both sites are used simultaneously.

TABLE I. Concentration dependent peak absorption coefficients α_0 [cm^{-1}] and inhomogeneous linewidth Γ_{inh} [GHz] at T = 2 K in Eu^{3+}:Y_2SiO_5. The D1, D2, and b axes are the main polarization axes. The Γ_h are the FWHM from Lorentzian fits to the absorption lineshapes.

	Site 1				Site 2			
Eu^{3+}	α_0 (D_1)	α_0 (D_2)	α_0 (b)	Γ_{inh}	α_0 (D_1)	α_0 (D_2)	α_0 (b)	Γ_{inh}
1 %*	2.8	0.6	0	32	0.9	0.2	1.0	39
0.5 %	3.1	0.6	0	11	1.3	0.2	1.3	12
0.1 %	3.8	1.0	0	1.7	1.7	0.3	2.2	1.4
0.01 %*	2.4	0.5	0	0.6	1.1	0.2	1.3	0.5

* grown from crystalline Y_2SiO_5 (all other crystals are grown from oxide powders)

The $^5D_0$ fluorescence lifetimes of 1.9 ms for site 1 and 1.6 ms for site 2. They were nominally independent of temperature.

From the list of parameters given above, two key parameters for optical data storage and processing using coherent transients or spectral hole burning are the optical homogeneous linewidth Γ_h and the optical inhomogeneous linewidth Γ_{inh}. The ratio Γ_{inh} / Γ_h is a measure of the potential storage density enhancement achievable through using the frequency selectivity of the optical material. The optical dephasing time T_2 limits the duration of data pulse sequences in some implementations of time-domain optical memories and is related to the homogeneous linewidth by $T_2 = 1/(\pi\Gamma_h)$. The T_2 was measured by two-pulse photon echo measurements. The optical dephasing times of T_2 = 2.6 ms, corresponding to a homogeneous linewidth of Γ_h = 122 Hz optical linewidths and optical Q > 4 X 10^{12}. The potential storage density enhancement factor is Γ_{inh}/Γ_h, = 10^7. Results for 2 K are summarized in Table II.

TABLE II. Homogeneous linewidth Γ_h [Hz] and storage density Γ_{inh} / Γ_h in Eu^{3+}:Y_2SiO_5 at T = 2 K.

	Site 1		Site 2	
Eu3+	Γh	Γinh / Γh	Γh	Γinh / Γh
1 %	1400	$2 \cdot 10^7$	2240	$1.6 \cdot 10^7$
0.5 %	360	$3 \cdot 10^7$	1500	$8 \cdot 10^7$
0.1 %	240	$7 \cdot 10^6$	410	$3 \cdot 10^7$
0.01 %*	260	$2 \cdot 10^6$	300	$2 \cdot 10^6$

* grown from crystalline Y_2SiO_5 (all other crystals are grown from oxide powders)

Thermally induced optical dephasing was measured for crystal temperatures from 2 K to 11 K and the expected T^7 dependence associated with Raman scattering of phonons was clearly observed, with a low temperature limit of $\Gamma_h \approx 120$ Hz for both the 0.01 and 0.1% Eu^{3+}:Y_2SiO_5 crystals.

At low temperatures the homogeneous linewidth does not change significantly with Eu^{3+} concentration and lies between 240 Hz and 2.2 kHz. At elevated temperatures, the phonon contribution starts to dominate the optical dephasing due to the onset of the T^7 behavior. For example, the homogeneous linewidth broadens to 10 kHz at 7.4 K for site 1 and at 9.1 K for site 2 for all samples. Above these temperatures, the homogeneous linewidths for all samples were nominally the same, independent of the Eu^{3+} concentration. At low temperature the potential storage density enhancement factor Γ_{inh} / Γ_h lies between $2 \cdot x\ 10^6$ at 0.01% and $8 \cdot x\ 10^7$ at 1%. At 7.4 K the storage density lies still between $5 \cdot x\ 10^4$ at 0.01% and $3 \cdot x\ 10^6$ at 1% for site 1. For site 2 the same storage densities are reached at 9.1 K.

The lifetime of the spectral holes measures the storage time of the optical hole burning memory, and it depends strongly on the temperature, with applications possible over both long and short storage times. For site 1, which had the longest lifetimes, the hole decay times were measured to be > 23 days at 2 K, 8 hours at 8 K, and 1 sec. at 15 K. The hole lifetime was independent of the Eu^{3+} concentration from 0.01% to 1%. Multiple components of the hole decay were observed due to the different spin-lattice relaxation rates between different hyperfine levels and two Eu isotopes. A measured decay for site 2 at 10 K is illustrated in Fig. 6.

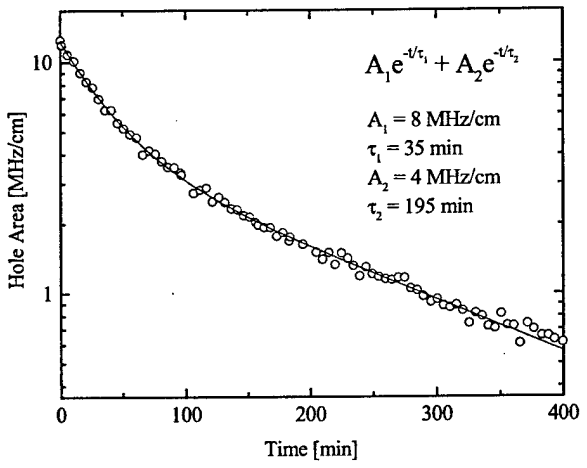

FIG. 6. Spectral hole persistence measured at 10 K in 0.1% Eu^3+:Y_2SiO_5 on site 2. The decay of the hole area shows at least two different relaxation rates associated with the three hyperfine components and two isotopes of Eu^{3+}. The solid line shows the fit of a double exponential function to the data.

The energy levels of all ^7F_J multiplets were determined from 1% Eu^{3+}:Y_2SiO_5 along with the inhomogeneous linewidths of levels within 50 cm^{-1} of the lowest level of each J multiplet. This is the first determination of the $^7F_3$ through $^7F_6$ level positions.

The purity of Eu^{3+}:Y_2SiO_5 crystals has a significant influence on their optical properties. The homogeneous linewidth measurements were sensitive to crystal impurities at concentrations of parts per million and are proposed as a powerful tool for investigating the purity and quality of these and other optical crystals.

Er^{3+} Materials for All-Optical Signal Processing, Data Switching and Routing, Buffer Memories, and other Network, Memory, and Optical Interconnect Devices in the 1.5 μm Communication Band

A broad goal of our material development work was to provide materials that enable all-optical data switching and routing, buffer memories, and other network, memory, optical interconnect, and signal processing devices and to provide highly parallel data transmission. This wavelength requirement is met by crystals containing Er^{3+}, and SHB systems development using these materials can exploit the broad range of optical components already existing in the 1.5 μm communications band such as fiber amplifiers, splitters, combiners, and modular detectors and/or can be integrated into larger systems.

Emphasis in the development of Er^{3+} materials was placed on refinement and characterization of Er^{3+}:Y_2SiO_5, Er^{3+}:Y_2O_3, Er^{3+}:KTP, Er^{3+}:YAG, and Er^{3+}:$LiNbO_3$. Other materials studied included Er^{3+}:$YAlO_3$, Er^{3+}:$CaWO_4$, Er^{3+}:$SrWO_4$, and Er^{3+}:CaF_2:D^-, for a total of nine materials.

The Er^{3+}:Y_2SiO_5 material enabled our demonstration of optical signal processors and will be used by other groups in Spectrum Lab at MSU and likely by other SHB device development groups. Demonstration of buffer memories at 1.5 μm is projected. The Er^{3+}:$LiNbO_3$ material offers several hundred GHz bandwidths and time-bandwidth products as large as 10^8.

These Er^{3+}-doped materials were all characterized by

- Site selective absorption and emission measurements on the $^4I_{15/2} \leftrightarrow {}^4I_{13/2}$ transitions to determine the inhomogeneous linewidths Γ_{inh}, the absorption coefficients α, the energy levels of each multiplet, and to ensure that crystal splittings were large enough to reduce optical dephasing by phonon processes.
- Measurements of the fluorescent lifetime T_1 of the lowest $^4I_{13/2}$ levels,
- Two-pulse photon echo measurements of the homogeneous dephasing times T_2 and homogeneous linewidths Γ_h,
- Electronic Zeeman effects and g-factors of the echo transitions and angle-dependent Zeeman measurements,
- Spectral diffusion measurements using stimulated photon echo measurements.

These experimental measurements were carried out as a function of applied magnetic field and Er^{3+} concentration, and temperatures were varied over the liquid helium temperature range and somewhat above.

Several tunable diode lasers were constructed in our laboratory for these measurements; an external cavity design refined by our group in collaboration with others at MSU was used with special angle-faceted laser diodes. The lasers produce 7 mW of single frequency output over a broad single-mode-tuning range. Two erbium-doped fiber amplifier were used to amplify laser output to ~50 mW or up to 1 W for some of the two-pulse and three-pulse photon echo experiments, but in many cases, a few mW of laser power was adequate even for these nonlinear experiments. These single-mode laser systems also enabled us to make high resolution determinations of the inhomogeneous widths Γ_{inh} for each material and of the energy level structure.

Optical dephasing and spectral diffusion were studied for the $^4I_{15/2} \leftrightarrow {}^4I_{13/2}$ transition of Er^{3+} at 1.5 μm in eight of these crystal systems. The Er^{3+} ions initially were doped into each crystal at very low concentration (~ 10 parts per million) to minimize optical dephasing and spectral diffusion. These measurements allowed us to show that the dominant dephasing and spectral diffusion mechanisms were Er^{3+}-Er^{3+} interactions; those range-dependent interactions lead to mutual electronic spin flip-flops of the Er^{3+} ions. There were observable effects also present due to interaction of the nuclear magnetic moments of neighboring ligand ions with the optically active Er^{3+} ions. Studies were then made to explore the practical ranges of Er^{3+} concentration.

All of the oxide crystals that we have studied were grown by Scientific Materials except for Er^{3+}:$LiNbO_3$, but Scientific Materials are now growing Er^{3+}:$LiNbO_3$ as well. Crystal design was a joint effort of our laboratory and Scientific Materials.

Desirable features for signal processing and for buffer memories include long T_2 for storing or processing long pulse trains, low spectral diffusion, and convenient wavelengths. To obtain long optical T_2 (corresponding to narrow Γ_h), a magnetic field is needed to split the Kramers doublet Er^{3+} electronic levels and minimize spin-flip-induced dephasing for photon echo and hole burning applications. It has been possible to achieve realistic values of T_2 using small button-sized permanent Nd-Fe-B magnets that provided fields of 2.5 kG. More optimized designs will produce far higher fields to several tens of kG. In these fields the 0.001% Er^{3+}:Y_2SiO_5 crystal gave $\Gamma_h \sim 2.5$ kHz. These experimental conditions were well suited to the device demonstrations that we have performed, and the button magnets were used in both of the demonstrations described in Section A above..

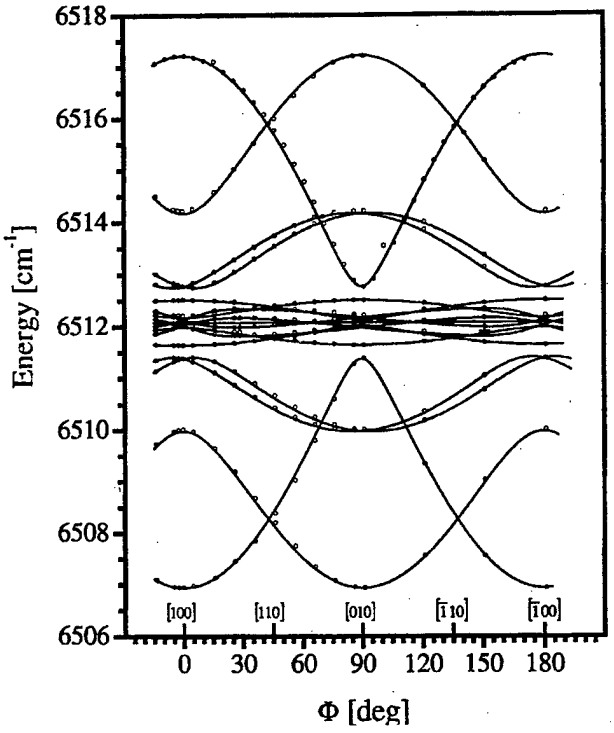

Fig. 7. Orientation dependence of the electronic Zeeman effect for the C_2-symmetry sites of Er^{3+}:Y_2O_3 at an applied field of 1.0 T. The open circles are data points and the lines are fits to the data. The square brackets label crystal symmetry directions.

To further optimize the materials, the anisotropy of the electronic Zeeman splittings have been exploited. This required measurement of the full angular dependence of the Zeeman effect for the echo transitions of all sites, since the ground state Er^{3+} levels are important for both sites. As an illustration of the range of measurements carried out on several crystals, the data for one plane of the C_2-symmetry sites of Er^{3+}:Y_2O_3 is shown in Fig. 7.

Symmetry Considerations Regarding Light Propagation and Light Polarization for Coherent Interactions with Ions in Crystals, Y. Sun, G. M. Wang, R. L. Cone, R. W. Equall, and M. J. M. Leask, Phys. Rev. B **62**, 15443-15451 (2000).

Optical signal correlators based on spectral hole burning and a broad variety of other optical-electronic applications as well as many spectroscopic techniques are based on the coherent interaction of optical radiation fields with ion-doped or molecular crystals of various types. The interactions include optical coherent transients, spectral hole burning, and spatial-spectral holography or time- and space-domain holography. Devices based on these concepts are useful in optical data storage, real-time optical signal processing, and optical data routing and have applications including computers, communications networks, the internet and other networks, optical correlators, true time delays in radar, and numerous other applications.

In this work, we optimized the *generated optical coherent transient signals for materials of any crystal structure – encompassing every possible crystalline material.* Typically, before our analysis, coherent signals with several time dependences would be generated in most materials, and the interference of those signals reduced the efficiency and time resolution in device applications and the sensitivity and effectiveness of the spectroscopic techniques.

General symmetry principles were used to find light field directions that guaranteed both an optimum single-Rabi-frequency interaction and the most efficient coherent transient generation in arbitrary crystals.

We accomplished this for all actual and potential crystal lattice symmetries found in all possible natural and synthetic optical materials. For all physically possible combinations of space group and point group symmetries, we showed that light propagation and polarization directions exist that provide a so-called *single-Rabi-frequency* temporal behavior. That is, for these special directions, *all of the active ions in the crystal are coherently driven and coherently radiate in phase.* This provides a much more ideal coupling between the ions and the radiation field and consequently a cleaner and faster transient response. (The optical Rabi frequency is given by $\Omega = \boldsymbol{p} \cdot \boldsymbol{E_0} / \hbar$ where $\boldsymbol{p}$ is the electric dipole moment with components $p_i = \langle 1 | p_i | 2 \rangle$ and $\boldsymbol{E_0}$ is the optical electric field vector. Similar expressions apply for magnetic dipoles and magnetic optical fields. The Rabi frequency is determined not only by the magnitudes of the transition dipole moment and of the optical field, but also by the projection of one onto the other.)

This theoretical analysis was applied experimentally to a wide range of rare earth crystals, many of which are important for technological applications. Single-Rabi-frequency optical nutation, illustrating the efficacy of this strategy, has been observed for Pr^{3+}:Y_2SiO_5, Tm^{3+}: $Y_3Al_5O_{12}$, and the Er^{3+} $^4I_{15/2}$ (1) – $^4I_{13/2}$ (1) transition in Er^{3+}:$YAlO_3$, Er^{3+}:$LiNbO_3$, Er^{3+}:$CaWO_4$, Er^{3+}:$SrWO_4$, Er^{3+}:Y_2O_3, Er^{3+}: $Y_3Al_5O_{12}$, and Er^{3+}:Y_2SiO_5.

Site interference in optical nutation of the SHB material Tm^{3+}:$Y_3Al_5O_{12}$ (Tm^{3+}:YAG) provided a direct illustration of what happens with and without this effect. Figure 8 shows the spatial relationships of the six crystallographically equivalent but orientationally inequivalent Y^{3+} or Tm^{3+} sites in Tm^{3+}:YAG. Two special light polarization directions <111> and <001> were found where the $^3H_6$ (1) to $^3H_4$ (1) transition dipoles of all Tm^{3+}sites excited by the light field $\boldsymbol{E}$

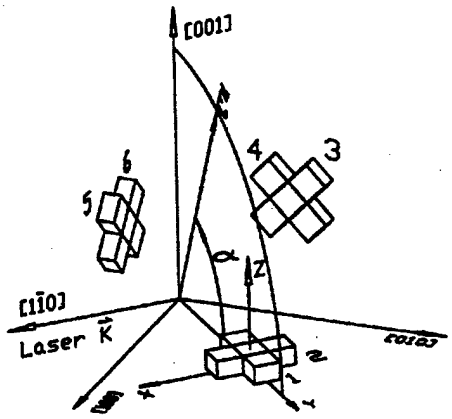

Fig. 8. Orientations of the six orientationally-inequivalent sites of the Y^{3+} ion in the yttrium aluminum garnet crystal lattice. Each lozenge-shaped parallelepiped represents the local D_2 symmetry for a subset of sites. The x, y and z axes are the local axes for site 1. Experiments were carried out with the light passing along the [1 $\bar{1}$0] axis and the light polarization was rotated from [110] to [001], and α is the angle between $\boldsymbol{E}_0$ and [110].

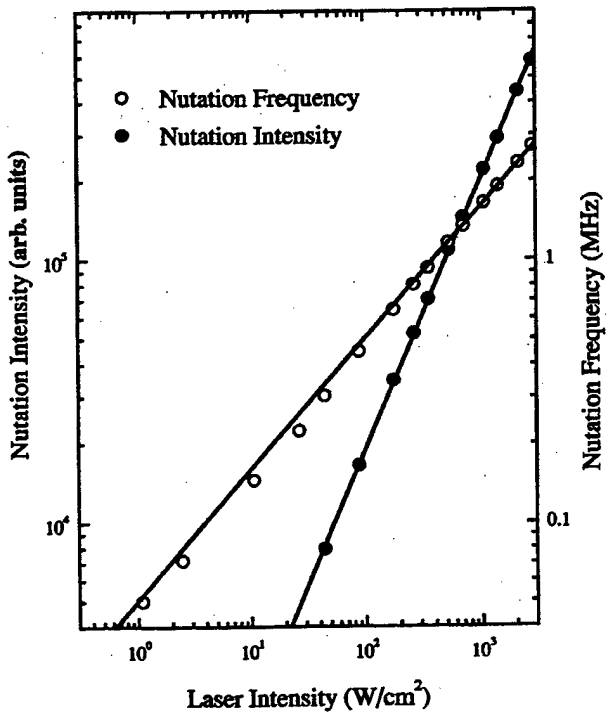

project equally onto the electric field vector. The optical nutation signals then exhibited the desired cooperative properties under coherent illumination. For other polarizations, complicated irregular optical nutation signals were observed due to the interference of the different frequency components from several sites in the crystal; all of the undesirable cases were also quantitatively explained.

The laser intensity dependence of the measured nutation signals was checked over 3 and a half decades, and the nutation frequency and signal intensity were both found to vary exactly as expected, as shown in Fig. 9.

A sample measured nutation signal along with a fit of the signal is shown in Fig 10, demonstrating that our model of this process gives good agreement. Figure 11 shows the variation of the measured and calculated nutation signals for various polarizations with light propagating along the degradation of the [1 $\bar{1}$0] direction. As we can see from this graph, a misalignment of only a few degrees can make a dramatic difference in the temporal behavior of the nutation signal. For the non-ideal directions, the amplitude is reduced and complex beating is present.

Fig. 9 (at left). Laser intensity dependence of the nutation signal and nutation frequency. The incident laser intensity was varied over 3.5 decades. The signal changes linearly with the intensity while the frequency changes with the square root of the intensity.

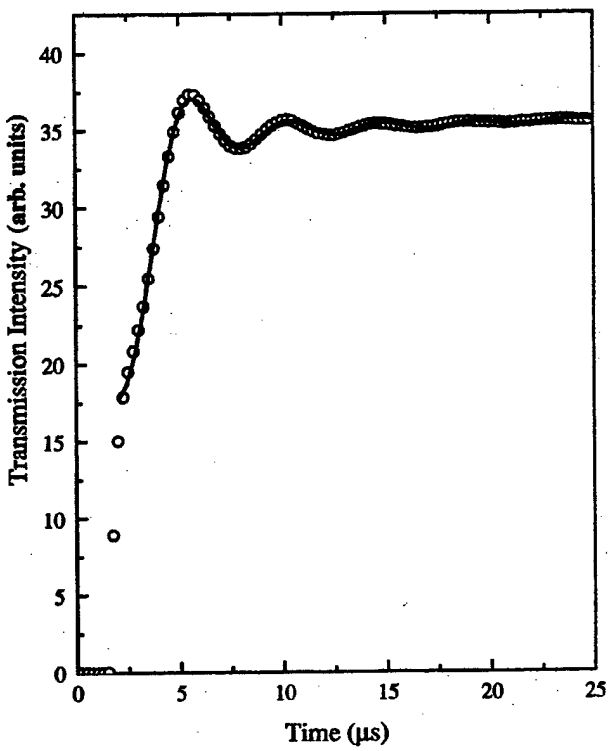

Fig. 10. Observed nutation signal of the $^3H_6$ (1) $\rightarrow$ $^3H_4$ (1) transition of 0.1% Tm^{3+}:$Y_3Al_5O_{12}$ for a laser propagating along the [1 $\bar{1}$0] direction and polarized along [111]. The incident power was ~26.3 W/cm^2. The solid line through the data was a simulation.

As a further benefit, this procedure allows us to determine the electric dipole moment of the material. In many systems, the direction of the transition dipole may not be known relative to the local axes, and it is not easy to measure traditionally. Optical nutation provides a simple way to find this direction.

For Tm^{3+}:$Y_3Al_5O_{12}$ (YAG), the local D_2 site symmetry of the Tm^{3+} ions allows the transition dipole for the Tm^{3+} $^3H_6$ (1) to $^3H_4$ (1) transition and to be along the x, y, or z axis of local symmetry. Our quantitative comparison of experimental nutation frequencies for light polarized along different directions resolved this ambiguity and allowed determination of the orientation of the optical transition dipole moment to be along <110> for this Tm^{3+} transition. Our measurement and analysis of optical nutation also allowed quantitative determination of the magnitude of the transition dipole moment, and the value agreed to within 15% with that obtained from absorption experiments. Absolute measurement of transition moments with such precision is unusual.

In cases when the number density is not well determined, optical nutation provides an independent way to measure the oscillator strength. We have exploited that idea by combining

We combined this kind of nutation measurement with absorption measurements to allow determination of site occupancy in multi-site materials like Pr^{3+}:Y_2SiO_5 where mismatches in the size of the Y^{3+} and Pr^{3+} ions leads to unequal occupation by Pr^{3+} of the two Y^{3+}sites. Independent measurement of transition strengths and ion concentrations are made practical by this technique, and that leads to applications characterizing a broad range of rare earth optical materials including solid state laser materials. These ideas for material characterization can thus be used to provide feedback to crystal growers for optimizing a broad range of optical devices from our correlators to solid state lasers.

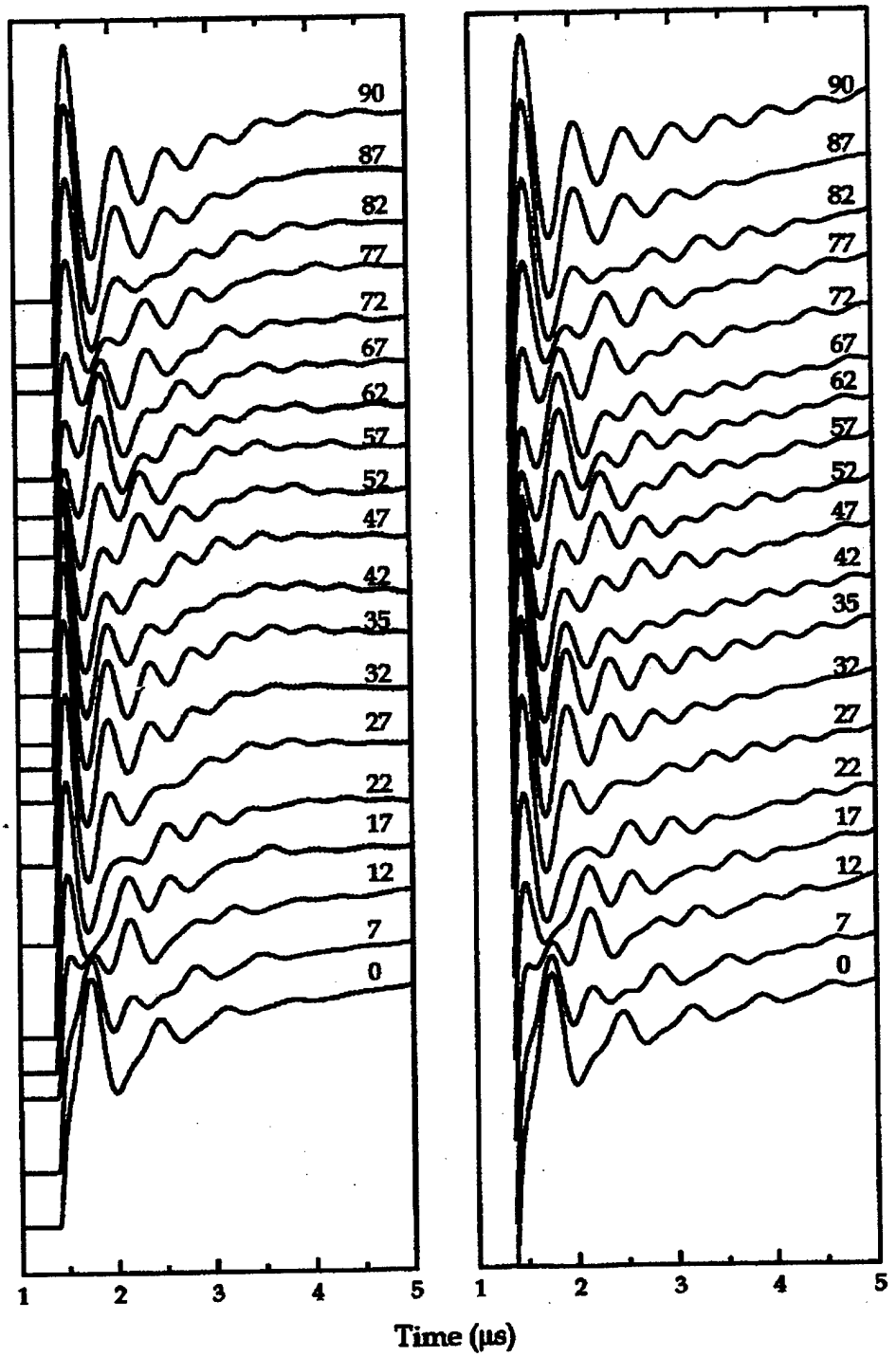

Fig. 11. On the left side are the observed optical nutation signals for the $^3H_6$ (1) $\rightarrow$ $^3H_4$ (1) transition of 0.1% Tm^{3+}:$Y_3Al_5O_{12}$ with the laser propagating along the [110] direction. The laser intensity on the crystal was 1.76 x 10^3 W/cm^2. The number above each trace is the angle α between $\boldsymbol{E}_0$ and [110]. On the right side are the calculated nutation curves for the same angles. The calculation used experimental parameters fitted only for the two directions $\boldsymbol{E}_0$ || [111] ($\alpha = 35.3°$) and $\boldsymbol{E}_0$ || [001] ($\alpha = 90°$). All other nutation signals were calculated without further fitting.

New Gated Spectral Hole Burning Materials

A variety of materials with various hole lifetimes – spanning many orders of magnitude – are needed for varied SHB applications. To provide long lived holes , we explored new materials and materials concepts for photon gating of persistent spectral hole burning. In this case selective excitation within an inhomogeneously broadened absorption line is the first step of a two-photon process, and hole burning only occurs when both the 'burning' and 'gating' photons are present simultaneously. As a consequence, continued exposure of the material to only burning photons does not modify the previously established hole pattern or shape. The "robustness" and long-term persistence associated with photon gating are important to some storage and signal processing applications and are especially important to SHB frequency standard and optical clock applications.

To extend photon gating to new systems, we have studied materials where photoionization of Tb^{3+} to Tb^{4+} can open new areas of study and offer material systems for operation in the blue spectrum, where future development of optical storage systems is expected. Specifically, we have carried out spectroscopic studies of Tb^{3+}:$LiYF_4$, Tb^{3+}:$LuPO_4$, Tb^{3+}:$ScPO_4$, Tb^{3+}:YPO_4, Tb^{3+}:YAG, Tb^{3+}:Y_2SiO_5, Tb^{3+}:$Y_2Si_2O_7$, and Tb^{3+}:$YAlO_3$. Both visible and ultraviolet absorptions studies were completed, along with some characterization of the excited state absorption spectra. There are a number of reasons for exploring terbium. The Tb^{3+} ion has the lowest energy 4f to 5d transitions of any rare earth ion, so both the hole burning and gating could be carried out with visible light. The terbium ion also exists in both the Tb^{3+} and the Tb^{4+} ionization states. Our photoemission studies, described below, highlight Tb^{3+} as one of the most favorable ions in terms of location of the Tb^{3+} ionic levels relative to the valence and conduction bands. Prospects for photon gated hole burning in the terbium system were pioneered in these studies of photon gated hole burning in rare earth materials. We had previously reported hyperfine hole burning in Tb^{3+}:$LiYF_4$ with hole lifetimes of minutes. Hole burning was observed during this project in Tb^{3+}:$YAlO_3$ and Tb:YAG. A new frequency doubled diode laser operating at the 488 - 489 nm region was employed in these experiments.

Our most important conceptual and experimental progress on photon gating involved a broad systematic experimental study and analysis of the positions of the tightly bound ionic states of all rare earth ions relative to the band states of the host material. These are described below in detail and in a paper that we believe will become a classic reference in the field of rare earth materials. Other experiments developed in our laboratory for gating studies included new ultraviolet absorption and photoconductivity experiments.

Systematics of 4f Electron Energies Relative to Host Bands by Resonant Photoemission of Rare Earth Ions in Aluminum Garnets, C. W. Thiel, H. Cruguel, H. Wu, Y. Sun, G. J. Lapeyre, R. L. Cone, R. W. Equall, and R. M. Macfarlane, Phys. Rev. B **64**, 085107 (2001) 13 pages.

To provide information needed for designing gated hole burning materials, the energies of trivalent rare earth ions relative to the host valence band were measured for a series of rare earth doped yttrium aluminum garnets, $R_xY_{3-x}Al_5O_{12}$ (R=Gd, Tb, Dy, Ho, Er, Tm, Yb, Lu and $0 \leq x \leq 3$), using ultraviolet photoemission spectroscopy. The 4f photoemission spectra were acquired using synchrotron radiation, exploiting the 4d to 4f "giant resonance" in the 4f electron photoemission

cross-section to separate the 4f contribution from the contribution of the host valence band. Theoretical valence band and 4f photoemission spectra were fit to the experimental results to accurately determine electron energies. The measured $4f^n$ ground state energies of these ions range from 700 meV above the valence band maximum for Tb^{3+} to 4.7 eV below the valence band maximum for Lu^{3+}, and all ground state energies, except for Tb^{3+}, were degenerate with valence band states. An empirical model was successful in describing the relative positions of the $4f^n$ ground states for different rare earth ions in these materials. This model was also used to estimate the positions of the lighter rare earth ions, giving good agreement with published excited state absorption and photoconductivity measurements on Ce^{3+} in yttrium aluminum garnet. It was also shown that the energies of the 4f electrons relative to the valence band can be estimated from the photoemission spectrum of the undoped host, providing a simple method for extending these results to related host crystals. The success of the model suggests that further studies of additional host compounds will rapidly lead to a broader picture of the effect of the host lattice on the 4f electron binding energies.

Our systematic study of the positions of $4f^n$ levels relative to the host band states for rare earth ions in a range of materials is needed to improve the understanding of interactions between these two very different types of electronic states and to allow models with predictive power to be developed and refined.

In addition to gated hole burning, interactions between rare earth ions and host band states lead to phenomena important for understanding basic material properties and developing a complete picture of the electronic structure of rare earth doped insulators. In particular, charge transfer between the rare earth ions and the host can lead to broad absorption bands in the visible or ultraviolet regions of the spectrum, possibly resulting in generation of color centers in the lattice. Because the strength of a charge transfer transition depends on the spatial overlap between the initial and final electronic states, intense charge transfer absorption bands may appear in the ion's excited state absorption spectrum even when no corresponding feature is observed in the ground state absorption spectrum. Host band states may also influence the atomic transitions of the ion itself by inducing broadening and an increase in transition probability for forbidden transitions through hybridization, while interactions between the band states and the 4f electrons also provide a mechanism for energy transfer, non-radiative relaxation, and nonlinear optical effects. These processes are all of fundamental physical interest since they represent coupling between the two extremes of highly localized and strongly correlated 4f electrons of the rare earth ion and de-localized one-electron band states of the host crystal.

In solid-state laser materials, transitions from excited states of rare earth ions to the conduction band of the host lattice can cause a parasitic absorption that overlaps lasing wavelengths, resulting in crystal heating, reduction of both gain and tuning range, and may completely inhibit laser action, as for Ce^{3+} and Pr^{3+} in yttrium aluminum garnet (YAG). Excited state absorption can also create color centers and optical damage and is the dominant reason for the failure of otherwise promising tunable blue and ultraviolet laser materials. In contrast, ionization can be beneficial for applications such as proposed optical memories, optical processors, and frequency standards based on photorefractive effects or photon-gated photoionization hole burning, which may employ controlled ionization of the rare earth ions for non-volatile data storage and processing. The radiation hardness of optical materials, which is essential for space based

applications, is strongly influenced by the energy of the rare earth ion relative to the host bands. In the particular case of YAG, some rare earth ions resist radiation damage, while others suffer damage through oxidation or reduction. The efficiency of scintillator and phosphor materials is influenced by the position of the $4f^n$ levels relative to the band states through both ionization of excited rare earth ions and energy exchange between band states and 4f electrons. In new luminescent materials for plasma and flat panel displays, the performance limitations of potential red and blue electroluminescent and phosphor materials may arise from field-induced or thermal ionization of the rare earth ions.

Photoemission spectroscopy offers several advantages over other techniques and can provide information that complements optical measurements. Photoemission allows the energies of both valence and atomic (core) electronic states to be directly determined relative to a common energy reference, whereas interpretation of optical methods such as excited state absorption and photoconductivity may be complicated by uncertainty regarding the nature of the initial and final states involved. We employed resonant photoemission to measure the binding energies of the 4f and valence band electrons for the series of rare earth ions from Gd^{3+} through Lu^{3+}, which allowed the 4f and valence band spectra to be separated and analyzed independently by exploiting resonances in the 4f photoemission.

Since very little was known about the effect of concentration on the relative energies of the $4f^n$ levels and band states, measurements were made for materials with rare earth concentrations ranging from pure YAG to the stoichiometric rare earth aluminum garnets. Our measurements indicate that the binding energies of both the valence band maximum (VBM) and rare earth ions are insensitive to the doping concentration to within an experimental accuracy of several hundred meV.

The process of photoemission involved ejection of electrons from the sample being studied and thus generated a positive charge in the sample. For the YAG samples studied, photoemission resulting from the applied ultraviolet light rapidly generated a potential on the sample that was large enough to prevent observation of direct photoemission. Differential charging was a source of broadening in the spectra and arose from several sources such as the irregular nature of the fractured surfaces, inhomogeneity in the light intensity over the focused spot, reduced probability for electron escape for ions further from the surface, and electric fields originating from regions of the crystal not directly illuminated. All of these effects were overcome in our experiments and analysis, and that allowed us to make precise comparisons between spectra.

One of the difficulties in measuring the position of the $4f^n$ levels using photoemission is that they often overlap the host valence band. This was overcome in our experiments by use of resonant photoemission to enhance the 4f contribution relative to that of the valence band.

The binding energies of the 4f ground state and the valence band maximum were measured for rare earth ions from Gd^{3+} to Lu^{3+} at atomic concentrations varying from 7% to 100%. Typical experimental spectra are given in Fig 12. Details of the analysis are given in the published paper cited at the beginning of this section.

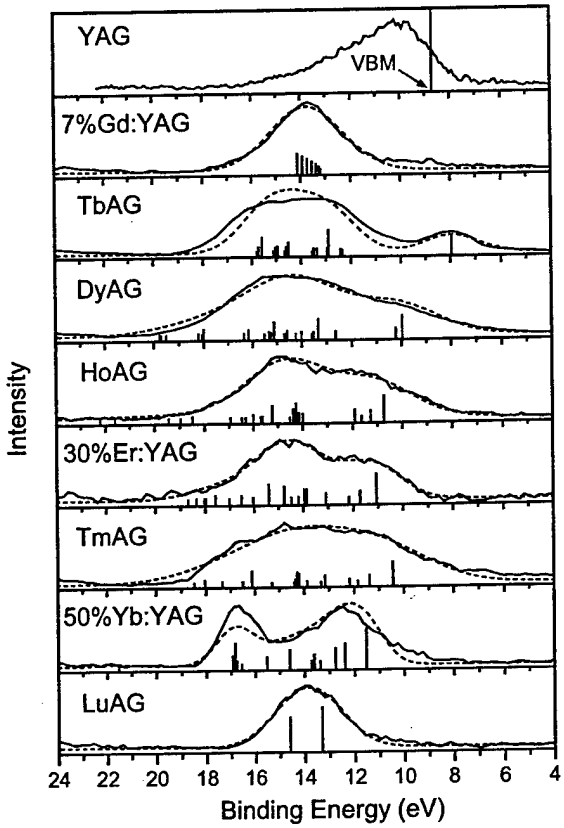

Figure 12. Representative data for each ion studied. Solid lines represent measured spectra with the secondary electron background subtracted and dotted lines are fits to the theoretical final state structure (see section IV). The vertical lines represent the underlying energy level structure. The valence band of YAG has been plotted for reference, with the position of the valence band maximum shown as a vertical line.

The conclusions from these measurements are summarized in Fig 13.

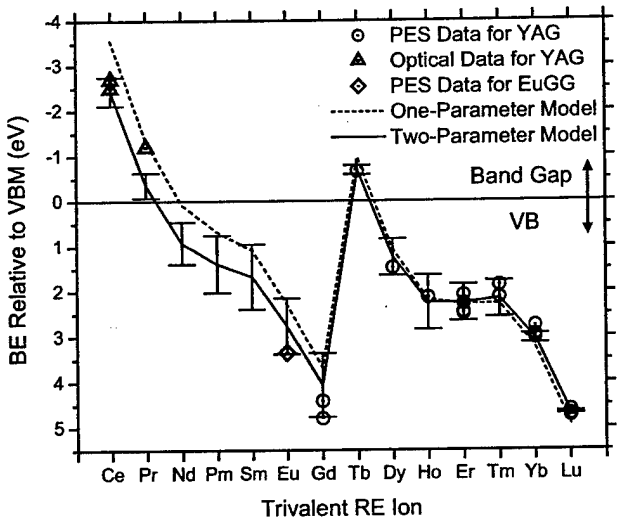

Figure 13. Systematic behavior of 4f binding energies relative to the valence band maximum. Circles represent our measured binding energies relative to the VBM (at 8.7 eV). The dotted line is the fit to our measured values without considering the effect of ionic radius. The solid line is the fit to our measured values including the effect of ionic radius. The error bars on the model are due to uncertainty in the values of the free-ion ionization potentials and the error bars on the extrapolated values for Eu^{3+} through Ce^{3+} include the uncertainty due to the accuracy of the fitting parameters. The triangles represent estimated positions from excited state absorption and photoconductivity measurements.

The relative positions of different trivalent rare earth ions shown in Fig. 13 are summarized in Table III. The binding energies ΔBE were successfully described by an empirical two-parameter model for the effect of the host crystal. This model describes the differences in binding energies of the rare earth ions as due to differences in free-ion ionization potentials, modified by a smaller effect due to the variation in ionic radii. Fitting the measured binding energies gave good agreement, with a 31.6 eV shift of the free-ion ionization potentials and an additional 8.3 eV/Å effect for the difference from the yttrium ionic radius. This model was supported by further comparison with energies obtained from published photoconductivity and excited state absorption measurements. The empirical model's success in describing the systematic trends in 4f binding energies indicates that measurements on two rare earth ions in the host may be sufficient to predict the energies of all other rare earth ions in that host, particularly if the accuracies of the free-ion ionization potentials used in the model are improved by further comparison with measurements.

As mentioned above, these studies are fundamental to developing gated hole burning materials and also provide important information for design of solid state laser materials – especially ultraviolet and radiation hardened materials, display phosphors, and scintillators.

Dopant Ion	*Concentration*	*ΔBE (eV)*
Gd	7%	4.8
Gd	100%	4.4
Tb	100%	-0.7
Dy	100%	1.5
Ho	100%	2.1
Er	30%	2.5
Er*	30%	2.3
Er	50%	2.5
Er	100%	2.1
Tm	10%	2.1
Tm	100%	1.9
Yb	10%	2.8
Yb	25%	3.0
Yb	50%	3.0
Yb	100%	3.0
Lu	50%	4.7
Lu*	70%	4.7
Lu	100%	4.6

*Measured in 30%Er:LuAG

Table III. Measured 4f electron ground state binding energies relative to the valence band maximum for all samples studied. Following the usual sign convention for binding energies, positive energies lie within the valence band and negative energies lie within the band gap.

Spectral Hole Burning and Optical Dephasing in Disordered Crystals – Pr^{3+}:$LiNbO_3$ and Pr^{3+}:$Sr_{.6}Ba_{.4}Nb_2O_6$ (SBN), R. M. Macfarlane, F. Könz, Y. Sun, and R. L. Cone, J. Lumin. **86**, 311-315 (2000).

With the goals of (a) providing broader lines with potential for greater device bandwidth, (b) providing new avenues for photon gating and photorefractive effects, and (c) generally broadening the scope of our material characterization, we have investigated materials that are structurally disordered. We measured the homogeneous line widths of the $^3H_4$ (1) to $^1D_2$ (1) transition of Pr^{3+} ions in the ferroelectric, photorefractive crystals, strontium barium niobate and lithium niobate. Spectral hole burning and photon echo experiments were carried out in the range 1.3 - 3 K. Both crystals show substitutional disorder and the presence of vacancies in the crystal lattice. A near-linear temperature dependence of the homogeneous line width was observed in both materials showing the presence of disorder modes or two-level systems (TLS). In the case of lithium niobate the density of states of the TLS is three orders of magnitude lower than in SBN and has not been detected in heat capacity measurements.

The low-temperature dynamical behavior of disordered materials such as glasses is largely determined by disorder modes or two-level systems (TLS), which determine the heat capacity and thermal conductivity as well as the line broadening of impurity centers through spectral diffusion and dephasing of spin and optical coherence. These modes have low frequencies of up to several cm^{-1} and are thought to involve collective motion of atoms or ions between almost equivalent configurations. There is also evidence from optical line width measurements, for the existence of TLS in some crystalline systems exhibiting disorder. The most characteristic signature of these modes is the presence of enhanced dephasing over that found in crystalline materials and an approximately linear dependence of the line width on temperature, in contrast to the case of ordered crystalline systems where an exponential or T^7 dependence is observed.

Since heat capacity is the classic method for detecting the presence of TLS it was interesting to measure optical line widths in systems for which heat capacity measurements have also been made. This has been done in the case of glasses where it was found that there was a correlation between the temperature dependences of the heat capacity and the optical line width. Here we report measurements of the temperature dependence of the optical line width of Pr^{3+} in two ferroelectric, photorefractive materials exhibiting disorder and for which heat capacity data are available. In the case of SBN the heat capacity is similar to that in glasses in showing a linear term at low temperatures and for lithium niobate the low temperature heat capacity shows a T^3, Debye-like temperature dependence characteristic of crystals.

In these materials the presence of a disordered lattice with numerous vacancies enhances the photorefractive effect by providing sites for dopants or intrinsic defects that act as sources and traps for charges. Our interest here is to investigate to what extent this disorder affects the low-temperature dynamical behavior of these materials as probed by the optical dephasing of Pr^{3+} ion dopants.

Two of these materials were studied. The crystals were grown by Dr R. R. Neurgaonkar.

The mixed crystal $Sr_{.6}Ba_{.4}Nb_2O_6$ (SBN60) belongs to the family of tungsten bronzes, of general formula $(A_1)_4(A_2)_2B_{10}O_{30}$ having a tetragonal space group P4bm with five formula units/unit cell. Site A_1 is partially occupied by Sr, and Sr,Ba are distributed in a disordered way over site A_2. The Nb sublattice on B sites is fully occupied and the oxygen sublattice shows vacancies disordered on the O positions. This high degree of disorder results in strongly inhomogeneously broadened lines. The $^3H_4$ (1) to $^1D_2$ absorption consists of four identifiable bands most of which show a polarized response, π at 16 498 cm^{-1}, $(\sigma + \pi)$ at 16 749 and 16 829 cm^{-1} and π at 17 047 cm^{-1}. The polarization behavior of the bands suggests that some lowering of the local site symmetry from C_{4v} has occurred because in axial symmetry the combination of π polarized and $\sigma + \pi$ polarized transitions from the same ground state level is not allowed. Since the inhomogeneous broadening is comparable to the expected crystal field splittings, it is possible that some of the broad lines contain unresolved crystal field components. However the lowest absorption line at 16 498 cm^{-1}, with a width of 90 cm^{-1}, corresponds to transitions between single electronic components since the emission and absorption spectra coincide over the full line width. Holes were burned in the 16 498 cm cm^{-1} line by irradiating with 100W/cm^2 for 10 s, and subsequently scanning the laser and recording a fluorescence excitation spectrum, detecting around 16 200 cm^{-1}. Data were taken under conditions where the hole width was independent of burning intensity. The background structure with a periodicity of 1 GHz is due to variations in the laser amplitude during the scan. The hole burning is typical of a glassy system in which the mechanism involves a local structural change, i.e., a TLS flip induced by the electronic excitation. The hole burning exhibits dispersive kinetics and saturates at about 20% depth indicating, as often happens in glassy systems, that some Pr^{3+} sites are much more easily photo bleached than others. This presumably reflects the variation in the probability of an optically induced TLS flip for ions in different sites. In addition, if the barriers are too low, thermal recovery occurs spontaneously and no bleaching occurs. These low-barrier TLS are the ones that produce a dynamic local strain field and are the source of line broadening. The hole-burning efficiency η, determined from the initial slope is ~10^{-6} which is typical for glassy systems as is the width of the holes, i.e., 220 MHz at 1.3 K, the recovery time of 100 min and the lack of observable anti-holes.

The temperature dependence of the hole width is linear in the range 1 - 4 K. This is characteristic of broadening by TLS with a constant density of states in this energy range and the magnitude of the broadening compared to that of Pr^{3+} in silicate glass for example, shows that this density of states is comparable to that of a true glass, i.e., about $10^{19}/cm^3$. Further confirmation comes from the measured heat capacity which has the form $C = AT + BT^3$ with $A = 2.5 \times 10^{-6}$ J/g K^2 compared to the value for Pr^{3+} in a silicate glass [14] of $A = 9.6 \times 10^{-6}$ J/g K^2.

The second material studied was Pr^{3+}:$LiNbO_3$. Lithium niobate has a rhombohedral structure with space group R3c and six formula units per unit cell. It has a considerably less disordered structure than SBN. The congruent composition is lithium deficient and the structure can be described in terms of a lithium vacancy model in which there are 4% Li vacancies, with 1% Nb_{Li} anti-sites providing charge compensation and the niobium and oxygen sublattices are fully occupied. Evidence from channeling shows that Pr^{3+} ions enter the Li sites that have nominally C_3 symmetry. It was proposed by Munoz-Santiuste et al. that charge compensation does not reduce this symmetry and that there are four discrete sites distinguished by the displacement of the Pr^{3+} ions along the *c*-axis. They further proposed that the lowest energy absorption to $^1D_2$ is

from a ground state doublet $^3H_4$ (E) to an excited state doublet $^1D_2$ (E).. In the C_3 axial symmetry model, the three main absorption features around 16 220, 16 420 and 16 600 cm^{-1} correspond to transitions to E, A, and E components, respectively. A closer look at the lowest group of lines shows four components at 16 183, 16 204, 16 245 and 16 266 cm^{-1}. We assign these to two partially resolved sites, S_1 at 16 183 cm^{-1} and S_2 at 16 204 cm^{-1} and transitions to components of the E level split by 62 cm^{-1}. The assignment to two sites is based on the fact that emission is not observed from the upper components at 16 245, 16 266 cm^{-1} at 1.3 K and on the photon-echo excitation spectrum mentioned below. This lowering of the symmetry shows that there are charge compensators off axis. The emission spectrum indicates the presence of a ground state level of energy ~65 cm^{-1} for the two sites.

Since the absorption and emission spectra show that the Pr site symmetry is lower than axial and hence that the ground and excited electronic states are electronic singlets separated by tens of cm^{-1} from the next singlet, we expect pseudo-quadrupole splittings of these levels to be some tens of MHz. The hole-burning mechanism for Pr:LNB is then different from that in Pr : SBN because the line widths are much narrower than the hyperfine splittings and optical pumping of the hyperfine levels occurs. This results in about four orders of magnitude higher burning efficiency ($\eta \approx 1\%$) and the observation of anti-holes. The hole spectrum is expected to consist of a central hole with two side holes at lower and at higher frequencies, the five holes not being resolved because of the laser frequency jitter of approximately 3 MHz over the hole-burning time together with inhomogeneous contributions to the width of the side holes. The spectrum of anti-holes is similarly broadened. Thus, the hole widths at 1.3 K do not reflect the intrinsic line width or optical dephasing rates. Hole recovery occurs because of spin-lattice relaxation between the hyperfine components and has a time constant of about 100 s.

Two-pulse photon-echo measurements were made by gating the cw dye laser with an acousto-optic modulator using a peak laser power of ~10 mW focused to a spot of 30 μm diameter in the crystal and the excitation pulses were 1 μs long. Data taken at higher laser intensity showed that instantaneous diffusion was not contributing to the measured decays. Echo decay times at 1.3 K were 4 μs. Echo excitation spectra were measured from 16 150 to 16 250 cm^{-1} and echoes were observed only for the two lowest lines at 16 183 and 16 204 cm^{-1} confirming that the upper two components at 16 245, 16 266 cm^{-1} arise from transitions to an excited electronic component for the two sites. The temperature dependence of the echo decay time ($T_2/4$) was measured between 1.3 and 3 K, and this showed that the homogeneous line width $\Gamma_h = 1/\pi T_2$ is nearly linear in temperature in this low-temperature range, being proportional to $T^{1.36 \pm 0.05}$. In addition, the absolute value of the line width is much larger than that typically found in crystalline environments with oxygen coordination [22]. This rather surprising result provides strong evidence for dephasing by disorder modes or TLS as observed in Pr:SBN, but the absolute line width and hence the density of TLS states is about three orders of magnitude lower. No linear term was found in heat capacity measurements of lithium niobate and for such a low density of states it would be difficult to detect. It appears that the optical dephasing of impurity center transitions can be a much more sensitive probe of the presence of TLS modes in crystalline materials than is heat capacity. It should be noted that there is another interesting possibility and that is that the Pr^{3+} impurity itself creates the TLS.

Both Pr in SBN and lithium niobate can be used to probe the thermal excitations at low temperature that are associated with their disordered structures. In Pr:SBN the hole-burning characteristics are glass like and the large line width of 110 MHz is attributed to TLS modes as expected from the substantial linear term in the heat capacity. In Pr:LNB, on the other hand, we found the surprising result that while hole burning was due to optical pumping of the hyperfine levels as in crystalline systems and the heat capacity showed a crystalline Debye-like behavior, optical dephasing was caused by a low density of TLS modes as shown by a near-linear temperature dependence between 1.3 and 3 K. The relationship between the nature of the disorder and the TLS density remains a central question in this field. It has been suggested by S. K. Watson that disorder associated with large strain fields may give rise to a high density of TLS.

PERSONNEL SUPPORTED AND ASSOCIATED

Several postdoctoral fellows and visiting scientists worked on this AFOSR research project. Dr. Flurin Koenz worked primarily on Eu^{3+} and Pr^{3+} materials including Eu^{3+}- and Pr^{3+}-doped Y_2SiO_5, $LiNbO_3$, and $Sr_{0.6}Ba_{0.4}Nb_2O_6$ (SBN). Dr. H. Wu and Dr. H. Cruguel of Professor Gerald Lapeyre's group assisted in the experimental study of the relationship of rare earth ion levels and host band structure by electron photoemission spectroscopy using synchrotron radiation; that work was targeted to development of gated spectral hole burning materials, and it has also lead to more general advances in understanding of rare earth doped optical materials applied to lasers, phosphors, and scintillators.

Cone's group has had the following graduate students involved in this AFOSR research project. Their salaries were paid by fellowships or by other research grants including DoD AASERT.

1) Todd Harris will complete his Ph.D. in Physics in May 2001. He developed analog optical signal processing device demonstrations at 1.5 μm using diode lasers (ECDL) and erbium doped fiber amplifiers (EDFA), and characterized Er^{3+} compounds for 1.5 μm devices in photon echo measurements. These demonstrations were of all-optical optical header decoders for packet switching and tests of code fidelity in all-optical correlators.
2) Charles Thiel was awarded an NSF graduate fellowship and will complete his Ph.D. in Physics in May 2002. Thiel worked on gated spectral hole burning materials and has carried out innovative UV electron photoemission spectroscopy that has allowed the design and selection of ideal candidate materials, many containing Tb^{3+} ions. This challenging work also has improved the general understanding of a wide range of other optical materials including lasers, phosphors for displays and illumination, and scintillators for imaging applications.
3) Gregory Reinemer will complete his Ph.D. in Physics in May 2002. Reinemer has characterized materials for spectral hole burning devices.
4) Thomas Bottger will complete his Ph.D. in Physics in May 2002. Bottger has applied our ultra-narrow band lasers, precisely stabilized to spectral holes, to studies of Er^{3+} spectral hole burning materials.
5) Sebastien Ermeneux completed his Ph.D. in October 1999 at the University of Lyon I, Lyon, France, after carrying out half of his thesis research in our laboratory. At our laboratory, Ermeneux studied the coherence properties of Nd^{3+}:YVO_4, showing that it is an optimum material for analog optical signal processing at infrared wavelengths due to its large oscillator strength. Ermeneux's visit was supported jointly by Scientific Materials Corporation and an NSF award. This is a continuation of our long interaction with the Laboratoire de Physico-Chimie des Matériaux Luminescents, Université Claude Bernard Lyon I, Lyon, France.

Cone's group had nine undergraduate students involved in AFOSR research during this grant period.

1) Glenn Omdahl, an undergraduate student in Physics, received his BS in Physics, in May, 1998, and began work for AFOSR SBIR Contractor, Scientific Materials Corporation.
2) Seth Mayer, undergraduate student in Physics, received his BS in Physics, in May, 2000.
3) Kevin Yager, an undergraduate student in Physics, received his BS in Physics, in May 2000.

4) Malina Schindel, undergraduate student in Physics was involved in electronic construction projects.

5) Andrew Schmidt, undergraduate student in Physics was involved in electronic construction projects.

6) Casey Dodge, Mechanical Engineering student, received his B.S. in Mechanical Engineering in May 2000. Dodge designed and built six external cavity diode lasers, using CAD/CAM techniques and CNC machines. This design has been reproduced by several other research groups funded by DoD.

7) Anna Hagenston, undergraduate student in Physics, will receive her BS in Physics, in May 2001. Ms. Hagenston won the Dean's Award for Excellence in the College of Letters and Science in May 2000.

8) Dustin Rich, Mechanical Engineering student, has fabricated diode lasers parts and designed other apparatus using CAD/CAM techniques and CNC machines.

9) Michael Patterson, undergraduate student in Physics, was involved in electronic construction projects.

PUBLICATIONS

1. *Demonstration of Real-Time Address Header Decoding for Optical Data Routing at 1536 nm*, T. L. Harris, Y. Sun, R. L. Cone, R. M. Macfarlane, and R. W. Equall, Opt. Lett. **23**, 636-638 (1998).

2. *Persistent Spectral Hole Burning in Deuterated CaF_2:Tm^{3+}*, N. M. Strickland, R. L. Cone, and R. M. Macfarlane, Phys. Rev. B. **59**, 14328-14335 (1999).

3. *Multiphonon Relaxation in YVO_4 Single Crystals*, F. S. Ermeneux, C. Goutaudier, R. Moncorgé, Y. Sun, R. L. Cone, E. Zannoni, E. Cavalli, and M. Bettinelli, Phys. Rev. B **61**, 3915-3921 (2000).

4. *Spatial-Spectral Holographic Correlator at 1536 nm Using 30-Symbol Quadriphase- and Binary-Phase-Shift Keyed Codes*, T. L. Harris, Y. Sun, W. R. Babbitt, R. L. Cone, J. A. Ritcey, and R. W. Equall, Opt. Lett. **25**, 85-87 (2000).

5. *Spectral Hole Burning and Optical Dephasing in Disordered Crystals – Pr^{3+}:$LiNbO_3$ and Pr^{3+}:$Sr_{.6}Ba_{.4}Nb_2O_6$ (SBN)*, R. M. Macfarlane, F. Könz, Y. Sun, and R. L. Cone, J. Lumin. **86**, 311-315 (2000).

6. *Symmetry Considerations Regarding Light Propagation and Light Polarization for Coherent Interactions with Ions in Crystals*, Y. Sun, G. M. Wang, R. L. Cone, R. W. Equall, and M. J. M. Leask, Phys. Rev. B **62**, 15443-15451 (2000).

7. *Systematics of 4f Electron Energies Relative to Host Bands by Resonant Photoemission of Rare Earth Ions in Aluminum Garnets*, C. W. Thiel, H. Cruguel,* H. Wu,† Y. Sun, G. J. Lapeyre, R. L. Cone, R. W. Equall, and R. M. Macfarlane, Phys. Rev. B **64**, 085107 (2001) 13 pages.

Manuscripts Prepared for Publication

1. *Er^{3+} Materials for Spectral Hole Burning and Optical Coherent Transient Devices,* Y. Sun, R. L. Cone, and R. W. Equall.

2. *Spectroscopy at 1.5 μm of Er^{3+} $^4I_{15/2}$ and $^4I_{13/2}$ Levels and Magnetic g-Tensors for $Er^{3+}:Y_2O_3$,* G. Reinemer, T. L. Harris, Y. Sun, R. L. Cone, and R. W. Equall.

3. *Photon Echo Characterization of the Electro-Optic Material Er^{3+} - doped KTP at 1.5 Microns,* G. Reinemer, T. Böttger, Y. Sun, and R. C. C. Ward.

4. *Concentration, Temperature, and Composition Dependence of Optical Dephasing, Spectral Hole Lifetime, and Anisotropic Absorption in $Eu^{3+}:Y_2SiO_5$,* Flurin Könz, Y. Sun, C. W. Thiel, R. L. Cone, R. W. Equall, R. L. Hutcheson, and R. M. Macfarlane.

5. *Tm^{3+} Materials for Spectral Hole Burning and Optical Coherent Transient Devices,* Y. Sun, R. L. Cone, and R. W. Equall.

6. *Site Occupancy Determination in $Pr^{3+}:Y_2SiO_5$ by Optical Nutation and Absorption,* Y. Sun, Flurin Könz, R. L. Cone, and R. W. Equall.

7. *Persistent Spectral Hole Burning in Deuterated $Er^{3+}:CaF_2$,* N. M. Strickland, R. L. Cone, R. M. Macfarlane, and G. D. Jones.

8. *Optical Coherence in Nd:YVO_4 by Photon Echo Spectroscopy,* Y. Sun, S. Ermeneux, R. L. Cone, and M. Bettinelli.

INTERACTIONS

A. Presentations and Participation at Meetings and Conferences

Invited Conference Talks

New Rare Earth Spectral Hole Burning Materials, Material Characterization, and Applications, Fourth International Workshop on Applications of Spectral Hole Burning, Montana State University, Bozeman, MT, March 9-11, 1998.

Advances in Rare Earth Crystals for Spectral Hole Burning Applications and Frequency References, R. L. Cone, Texas A&M – Office of Naval Research Quantum Optics Workshop, Jackson, Wyoming, August 2-6, 1998.

New Rare Earth Materials, Material Concepts, and Prototype Devices, R. L. Cone, Y. Sun, F. Könz, N. M. Strickland, T. L. Harris, C.W. Thiel, T. Böttger, G. Reinemer, and W. R. Babbitt, R. W. Equall and R. L. Hutcheson, R. M. Macfarlane, J. A. Ritcey, Fifth

International Workshop on Applications of Spectral Hole Burning, Montana State University, Bozeman, MT, March 7-10, 1999.

Plenary Talk, *Applications of Spectral Hole Burning,* R. L. Cone, First Meeting of the Northwest Section of the American Physical Society, Vancouver, BC, Canada, May 21 - 22, 1999.

Photon Echo Characterization of Er^{3+} Doped Oxide Materials at 1.5 μm, Y. Sun, R. L. Cone, T. L. Harris, R. M. Macfarlane, and R. W. Equall, 12th International Conference on Dynamical Processes in Excited States of Solids, Humacao, Puerto Rico, May 23 - 27, 1999.

Photon Echoes and Signal Processing Applications of Erbium Doped Oxides, Y. Sun, R. L. Cone, T. L. Harris, R. W. Equall, R. L. Hutcheson, R. M. Macfarlane, 22nd Rare Earth Research Conference, Argonne National Laboratory, Advanced Photon Source Conference Center, Argonne, IL, July 10 - 15, 1999.

Rare Earth Spectroscopy and Laser Frequency Stabilization to Ultranarrow Spectral Holes, R. L. Cone, Texas A&M – Office of Naval Research Quantum Optics Workshop, Jackson, Wyoming, July 26 - 30, 1999.

Rare Earth Spectral Hole Burning Materials, R. L. Cone, 1st Lyon Workshop on Nano-Optics, Universite Claude Bernard, Lyon, France, September 15 and 16, 1999.

New Rare Earth Materials, Material Concepts, and Demonstrations of Spectral Hole Burning Applications, R. L. Cone, Y. Sun, F. Könz, N. M. Strickland, T. L. Harris, C. W. Thiel, T. Böttger, G. Reinemer, W. R. Babbitt, R. W. Equall, R. L. Hutcheson, R. M. Macfarlane, and J. A. Ritcey, 6th International Conference on Hole-Burning and Related Spectroscopies, Hourtin, France, September 18 - 23, 1999.

Spectral Hole Burning for Laser Spectroscopy and Applications, R. L. Cone, La Societe Francaise de Physique, Section Rhone-Loire, Universite Lyon I, Lyon, France, September 30, 1999.

Lasers Stabilized to Spectral Holes and a Survey of Hole Burning Materials for Signal Processing, R. L. Cone, Laboratoire de Physico-Chemie Materiaux Luminescents, Universite Lyon I, Lyon, France, October 4, 1999.

Lasers Stabilized using Spectral Holes, P. B. Sellin, N. M. Strickland, J. L. Carlsten, R. L. Cone, 30th Winter Colloquium on The Physics of Quantum Electronics, Snowbird, Utah, January 9-12, 2000.

Characterization and development of new rare earth optical materials, Y. Sun, R. L. Cone, C. W. Thiel, T. L. Harris, T. Böttger, G. Reinemer, and R. W. Equall, 30th Winter Colloquium on The Physics of Quantum Electronics, Snowbird, Utah, January 9-12, 2000.

New Spectral Hole Burning Devices and Spectral Hole Burning Materials, R. L. Cone and Y. Sun, AFOSR Workshop, SRI, Menlo Park, California, May 25, 2000.

Rare Earth Materials for Lasers, Spectral Hole Burning and Stabilized Lasers, R. L. Cone and Y. Sun, Townes Festival 2000, Teton Village, Wyoming, July 31 - August 4, 2000

Plenary Talk, *Spectroscopy of rare earth materials from 20 Hz to hundreds of electron volts,* R. L. Cone, 31st Winter Colloquium on The Physics of Quantum Electronics, Snowbird, Utah, January 7-11, 2001.

Conference Organization and Session Chair

Session Chair, *M26 IMSTG: Near Field Microscopes – Optical*, March Meeting of the American Physical Society, Los Angeles, CA, March 15 - 20, 1998.

Session Chair, *O15 DCMP: Optical Properties -- Ions in Solids*, March Meeting of the American Physical Society, Los Angeles, CA, March 15 - 20, 1998.

Program Committee, 6th International Conference on Hole-Burning and Related Spectroscopies, Hourtin, France, September 18 - 23, 1999.

Session Organizer and Chair, *Rare Earth Materials,* 30th Winter Colloquium on The Physics of Quantum Electronics, Snowbird, Utah, January 9-12, 2000.

Session chair, *Session P-19, Insulators and Dielectrics, Defects and Spectroscopic Properties*, March Meeting of The American Physical Society, Minneapolis, MN, March 22, 2000.

International Organizing Committee, 13th International Conference on Dynamical Processes in Excited States of Solids / Conférence Internationale Dynamique des Etats Excités dans les Solides, Université Claude Bernard Lyon1, Lyon, France, July 1 - 4, 2001. Active in 2000.

International Organizing Committee, 7th International Conference on Hole-Burning, Single Molecule, and Related Spectroscopies, Taipei, Taiwan, November 18 – 23, 2001, sponsored by Institute of Atomic and Molecular Sciences, Academica Sinica, Taipei, Taiwan. Active in 2000.

Contributed Talks

Demonstration of Real Time Address Header Decoding for Optical Data Routing at 1536 nm, T. L. Harris, Yongchen Sun, R. L. Cone, R. M. Macfarlane, and R. W. Equall, Fourth International Workshop on Applications of Spectral Hole Burning, Montana State University, Bozeman, MT, March 9-11, 1998.

Er^{3+} Materials for All-Optical Switching and Routing at 1.5 μm, Y. Sun, R. L. Cone, T. L. Harris, R. M. Macfarlane, and R. W. Equall, March Meeting of the American Physical Society, Los Angeles, CA, March 15 - 20, 1998.

Tm^{3+} Materials for Coherent Transient Signal Processing Near 790 nm, R. L. Cone, G. M. Wang, Y. Sun, R. M. Macfarlane, March Meeting of the American Physical Society, Los Angeles, CA, March 15 - 20, 1998.

Persistent Spectral Hole Burning in CaF2:Tm^{3+}:D^-, N. M. Strickland, R. L. Cone, Physics Department, R. M. Macfarlane, March Meeting of the American Physical Society, Los Angeles, CA, March 15 - 20, 1998.

Advances in Rare Earth Crystals for Coherent Transient Applications and Lasers, R. L. Cone, Optical Science and Laser Technology Conference, Montana State University, Bozeman, MT, Aug. 17 - 18, 1998.

Temperature, Concentration, and Composition Dependence of Optical Dephasing in Eu^{3+}:Y_2SiO_5, Flurin Koenz, Yongchen Sun, and R. L. Cone, R. W. Equall and R. L. Hutcheson, Optical Science and Laser Technology Conference, Montana State University, Bozeman, MT, Aug. 17 - 18, 1998.

Demonstration of Real Time Address Header Decoding for Optical Data Routing at 1536 nm, T. L. Harris, Y. Sun, and R. L. Cone, R. M. Macfarlane, R. W. Equall and R. L. Hutcheson, Optical Science and Laser Technology Conference, Montana State University, Bozeman, MT, Aug. 17 - 18, 1998.

Terbium Compounds for Photon-Gated Persistent Spectral Hole Burning, C. W. Thiel, Y. Sun, R. L. Cone, R. W. Equall and R. L. Hutcheson, and R. M. Macfarlane, Optical Science and Laser Technology Conference, Montana State University, Bozeman, MT, Aug. 17 - 18, 1998.

Er^{3+} Materials for All-Optical Switching and Routing at 1.5 μm, Y. Sun, T. L. Harris, and R. L. Cone, R. M. Macfarlane, R. W. Equall and R. L. Hutcheson, Optical Science and Laser Technology Conference, Montana State University, Bozeman, MT, Aug. 17 - 18, 1998.

Holographic Detection of Persistent Spectral Holes and Demonstration of a Passive Optical Router at 1.5 microns, N. M. Strickland, T. L. Harris, and R. L. Cone, Optical Science and Laser Technology Conference, Montana State University, Bozeman, MT, Aug. 17 - 18, 1998.

Optical Spectroscopy of Defect Sites in Rare Earth Garnets, G. Reinemer, A. Hagenston, Y. Sun, G. M. Wang, and R. L. Cone, R. W. Equall and R. L. Hutcheson, and R. M. Macfarlane, Optical Science and Laser Technology Conference, Montana State University, Bozeman, MT, Aug. 17 - 18, 1998.

A Spatial-Spectral Holographic Correlator at 1536 nm using 30-Symbol BPSK and QPSK Codes Optimized for Secure Communications, T. L. Harris, Y. Sun, R. L. Cone, W. R. Babbitt, R. W. Equall, R. L. Hutcheson, and J. A. Ritcey, Fifth International Workshop on Applications of Spectral Hole Burning, Montana State University, Bozeman, MT, March 7-10, 1999.

Symmetry Considerations Regarding Light Propagation and Light Polarization for Coherent Interactions with Ions in Crystals, R. L. Cone, Y. Sun, G. Wang, and R. W. Equall, Centennial Meeting of the American Physical Society, Atlanta, GA, March 20-26, 1999.

Concentration, Temperature, and Composition Dependence of Optical Dephasing and Anisotropic Absorption in Eu^{3+}*:*Y_2SiO_5*,* F. Könz, Y. Sun, C. W. Thiel, R. L. Cone, and R. W. Equall, Centennial Meeting of the American Physical Society, Atlanta, GA, March 20-26, 1999.

Site Occupancy Determination in Pr^{3+}*:*Y_2SiO_5 *by Optical Nutation,* Y. Sun, F. Könz, R. L. Cone, and R. W. Equall, Centennial Meeting of the American Physical Society, Atlanta, GA, March 20-26, 1999.

A Spatial-Spectral Holographic Correlator at 1536 nm using 30-Symbol BPSK and QPSK Codes Optimized for Secure Communications, T. L. Harris, Y. Sun, R. L. Cone, W. R. Babbitt, J. A. Ritcey, and R.W. Equall, OSA Optics in Computing Conference, Snowmass, CO, April 12-16, 1999.

A Spatial-Spectral Holographic Correlator at 1536 nm Using 30 Symbol BPSK and QPSK Codes Optimized for Secure Communications, T. L. Harris, W. R. Babbitt, Y. Sun, R. L. Cone, J. A. Ritcey, and R.W. Equall, Conference on Lasers and Electro-Optics (CLEO), Baltimore, MD, May 23 - 28, 1999.

Advances in Hole Burning Materials, Optical Frequency Standards, and Lasers for Remote Sensing, R. L. Cone and Y. Sun, 1999 Optical Science and Laser Technology Conference, Montana State University, Bozeman, Montana, August 16-17, 1999.

A New Symmetry Principle Regarding Light Propagation and Light Polarization for Coherent Interactions with Ions in Crystals, Y. Sun, R. L. Cone, G. M. Wang, and R. W. Equall, 1999 Optical Science and Laser Technology Conference, Montana State University, Bozeman, Montana, August 16-17, 1999.

A Spatial-Spectral Holographic Correlator at 1536 nm using 30-Symbol BPSK and QPSK Codes Optimized for Secure Communications, T. L. Harris, Y. Sun, R. L. Cone, and W. R.

Babbitt, Physics Department, Montana State University, J. A. Ritcey, R. W. Equall, and R. L. Hutcheson, 1999 Optical Science and Laser Technology Conference, Montana State University, Bozeman, Montana, August 16-17, 1999.

Concentration, Temperature, and Composition Dependence of Optical Dephasing and Absorption in Eu^{3+}:Y_2SiO_5 for Optical Memory and Frequency Standards, F. Könz, Y. Sun, C. W. Thiel, R. L. Cone, R. W. Equall, R. L. Hutcheson, and R. M. Macfarlane, 1999 Optical Science and Laser Technology Conference, Montana State University, Bozeman, Montana, August 16-17, 1999.

Progress in Photoemission and Photoconductivity Measurements on Hole Burning Materials and Laser Materials, C. W. Thiel, Y. Sun, R. L. Cone, Herve Cruguel, G. J. Lapeyre, R. W. Equall, and R. M. Macfarlane, 1999 Optical Science and Laser Technology Conference, Montana State University, Bozeman, Montana, August 16-17, 1999.

Optical Spectroscopy of Defect Sites in Rare Earth Garnets, G. Reinemer, Y. Sun, G. M. Wang, R. L. Cone, R. W. Equall, R. L. Hutcheson, and R. M. Macfarlane, 1999 Optical Science and Laser Technology Conference, Montana State University, Bozeman, Montana, August 16-17, 1999.

Concentration and Temperature Dependence of Optical Dephasing and Hyperfine Spectral Hole Relaxation in Eu^{3+}:Y_2SiO_5, F. Könz, Y. Sun, C. W. Thiel, R. L. Cone, R. W. Equall, and R. L. Hutcheson, 6th International Conference on Hole-Burning and Related Spectroscopies, Hourtin, France, September 18- 23, 1999.

Persistent Spectral Hole Burning in Deuterated CaF_2:Tm^{3+} and CaF_2:Er^{3+} and Application to Laser Frequency Stabilization, N. M. Strickland, P. B. Sellin, J. L. Carlsten, R. L. Cone, and R. M. Macfarlane, 6th International Conference on Hole-Burning and Related Spectroscopies, Hourtin, France, September 18 - 23, 1999.

Homogeneous and Inhomogeneous Broadening of Rare-Earth Transitions in Lithium Niobate and Strontium Barium Niobate, R. M. Macfarlane, Y. Sun, T. L. Harris, R. L. Cone, and R. W. Equall, 6th International Conference on Hole-Burning and Related Spectroscopies, Hourtin, France, September 18 - 23, 1999.

Dephasing Processes Induced by Excited Ions in Pr^{3+}:Y_2SiO_5, S. Kröll, Baozhu Luo, R. W. Equall, F. Koenz, Y. Sun, and R. L. Cone, 6th International Conference on Hole-Burning and Related Spectroscopies, Hourtin, France, September 18 - 23, 1999.

Precision Optical Spectroscopy of Defect Sites in Rare Earth Garnets, G. Reinemer, G. M. Wang, Y. Sun, R. L. Cone, R. W. Equall, and R. L. Hutcheson, March Meeting of The American Physical Society, Minneapolis, MN, March 20-24, 2000.

Inhomogeneous and Homogeneous Broadening in Pr^{3+} and Er^{3+} Doped Lithium Niobate, R. M. Macfarlane, F. Könz, Y. Sun, T. L. Harris and R. L. Cone, Conference on Lasers and

Electro-Optics, Conference on Lasers and Electro-Optics, San Francisco, CA, May 7 - 12, 2000 #CThM59.

Optical Spectroscopy of Perturbed Sites in Rare Earth Garnets, G. Reinemer, G.M. Wang, C. W. Thiel, Y. Sun, R. L. Cone, R. M. Macfarlane, R. W. Equall, and R. L. Hutcheson, Northwest Section Meeting of the American Physical Society, Eugene, Oregon, May 19-20, 2000.

Stabilized Lasers and Hole Burning Materials, R. L. Cone, T. Böttger, G. J. Pryde, and N. M. Strickland, Workshop on Applications of Spectral Hole Burning 2000, Big Sky, Montana, July 9-12, 2000.

New Studies of Materials, Y. Sun, G. J. Pryde, C. W. Thiel, Flurin Könz, G. Reinemer, T. L. Harris, R. L. Cone, R. W. Equall, R. L. Hutcheson, Workshop on Applications of Spectral Hole Burning 2000, Big Sky, Montana, July 9-12, 2000.

Spectroscopy of Rare Earth Materials from 20 Hz to Hundreds of Electron Volts, R. L. Cone, Y. Sun, G. J. Pryde, .A. Braud, C. W. Thiel, T. L. Harris, T. Böttger, G. Reinemer, G. J. Lapeyre, R. W. Equall, and R. L. Hutcheson, 2000 Optical Science and Laser Technology Conference, Montana State University, Bozeman, Montana, August 14-15, 2000.

Systematics of Rare Earth Crystal Band Structure by Photoemission for Design of Laser and Hole Burning Materials, C. W. Thiel, Y. Sun, R. L. Cone, G.J. Lapeyre, and R.W. Equall, 2000 Optical Science and Laser Technology Conference, Montana State University, Bozeman, Montana, August 14-15, 2000.

Photon Echo Characterization in the Electro-Optic Material Er^{3+}:KTP at 1.5 Microns, G. Reinemer, T Böttger, Y. Sun, and R. L. Cone, 2000 Optical Science and Laser Technology Conference, Montana State University, Bozeman, Montana, August 14-15, 2000.

Rare Earth Spectroscopy, Materials for Spectral Hole Burning Devices, and Laser Frequency Stabilization to Ultra-Narrow Spectral Holes, R. L. Cone, T. Böttger, and G.J. Pryde, Atomic Physics Seminar, Physics Department, Yale University, October 27, 2000.

B. Consultative and Advisory Functions

Cone's group served as advisors on crystal design and characterization to Scientific Materials Corporation of Bozeman, MT, an AFOSR SBIR Phase II contractor. A number of new materials were developed and characterized in this role. Cone's group also worked to enhance linkage of Scientific Materials to other groups in the Spectral Hole Burning community. Together Scientific Materials and Cone's group served a primary role as material developers and providers for application and advancement of spectral hole burning technology.

These interactions included participation in yearly AFOSR Workshops:

- Fourth International Workshop on Applications of Spectral Hole Burning, Montana State University, Bozeman, MT, March 9-11, 1998.
- Fifth International Workshop on Applications of Spectral Hole Burning, Montana State University, Bozeman, MT, March 7-10, 1999.
- AFOSR Workshop, SRI, Menlo Park, California, May 25, 2000.

Advice was provided to Dr. W. Randall Babbitt, AFOSR grantee, on sensitivity of optical Rabi frequencies, optical nutation, and optical pulse areas to orientationally inequivalent sites in rare earth doped materials with complex crystal structures. Babbitt was advised on optimum geometries for correlator and true-time-delay applications that are based on spectral hole burning.

Our demonstration of single-Rabi frequency polarization conditions for Tm^{3+}:YAG has been important for the ONR MURI center in RF Photonic Systems for Arrays directed by Kelvin Wagner at the University of Colorado.

Professor Marlan Scully invited Cone to participate in the ONR/Texas A&M Workshops on Quantum Optics and Winter Colloquia on the Physics of Quantum Electronics. There is broad interest in rare earth materials for new quantum optical phenomena such as electromagnetically induced transparency, lasing without inversion, quantum information, and quantum computing.

Dr. Stefan Kroll of the U. of Lund, Sweden, and Cone's group have been collaborating on optical dephasing studies and submitted a proposal to the Swedish National Science Foundation. Kroll visited during March 1998 and March 1999.

Dr. R. M. Macfarlane of IBM Almaden Research Center visited our group for experiment collaboration on a number of occasions during March and April 1998 and March 1999.

Dr. Michael Jefferson of IBM Almaden Research Center visited for a week in January 1998 and a week in March 2000.

Dr. M. J. M. Leask of the Clarendon Laboratory, University of Oxford, visited our group for experiment collaboration for two weeks in March 1999.

Crystals of Er^{3+}:$KTiOPO_4$ (KTP) were grown and provided by Dr. R. C. C. Ward of the Clarendon Laboratory, University of Oxford.

There was regular electronic communication with both the IBM and Oxford groups throughout the project.

Dr. Jean-Louis LeGouet, Directeur de Recherche, Centre National de la Recherche Scientifique, Laboratoire Aime Cotton, Universite Paris Sud, Orsay, France, visited in 1998 and 1999.

Professor Richard Moncorgé of University of Caen, France, visited for a week in January 1998.

Professor Richard Meltzer of the University of Georgia visited for several days in January 1998.

Professor John Wright of the University of Wisconsin visited for several days in April 1998.

Dr. Neil Manson of the Laser Centre, Australian National University visited for a week in March 1999. Dr. Manson and Dr. Matt Sellars visited for a week in July 2000.

Professor Richard Chang of the Applied Physics Department, Yale University, visited for several days in October 1999.

Professor Rufus Cone visited the Laboratoire de Physico-Chimie des Matériaux Luminescents, Université Claude Bernard Lyon I, Lyon, France, for one month in September 1999.

Dr. W. R. Babbitt of the MSU Physics Department collaborated on the analog optical signal processing project for measuring the fidelity of correlator performance using phase shift keyed codes.

There were regular interactions with the interdisciplinary groups of the MSU Optical Technology Center (OpTeC).

C. Transitions:

We have developed and characterized a number of new spectral hole burning materials for optical correlators, memories, and other signal processing applications. With Scientific Materials we actively participated in the design of new materials. We cooperatively optimized the material properties through the close interaction with Scientific Materials made possible by our location; by providing rapid feedback. Adjustments were made to the synthesis process, leading to development of better quality materials.

The hole burning materials have been transferred to several other research groups at MSU, leading to significant advancements in their AFOSR and DoD funded programs:

- Professor W. R. Babbitt's group on optical signal processing has exploited the technology in sophisticated demonstrations of correlators and true-time delay generators and RF spectrum analyzer project.
- Dr. Kris Merkel and Alan Craig have used a Ti:S laser stabilized to spectral holes to demonstrate the accumulation of complex correlator signals for optical signal analysis.
- Groups in France, Sweden, and Australia have applied our materials and techniques in their development of optical correlators, memories, and RF spectrum analyzers.
- Scientific Materials Corporation provides the hole burning materials we have developed to the commercial market.

NEW DISCOVERIES, INVENTIONS, PATENT DISCLOSURES

The patent application process for a patent on new crystal optimization techniques is in progress. The title and abstract are:

Coherent Interaction of Optical Radiation Beams with Optical-Electronic Materials of Generalized Crystal Symmetry

A method for optimizing the interaction and propagation of a beam (or beams) of radiation through a material having generalized crystal symmetry includes determining a special direction relative to the axes of crystal symmetry of the material and polarizing the radiation beam along this direction. The polarized radiation beam is propagated through the material perpendicular to this special direction.

HONORS AND AWARDS

Charles Thiel, graduate student, was recipient of a National Science Foundation Graduate Fellowship. Earlier, as an undergraduate, Thiel had been a 1995 Congressional Barry M. Goldwater Scholar.

The Dean's Award for Excellence in the College of Letters and Science was presented in May 2000 to Anna Hagenston, an undergraduate who worked in our laboratory during summer 1998.

Dr. Yongchen Sun was promoted to Associate Research Professor from Assistant Research Professor.